

Follicular lymphoma-associated mutations in vacuolar ATPase ATP6V1B2 activate autophagic flux and MTOR

Fangyang Wang, ... , Daniel J. Klionsky, Sami N. Malek

J Clin Invest. 2019. <https://doi.org/10.1172/JCI98288>.

Research In-Press Preview Cell biology Oncology

The discovery of recurrent mutations in subunits of the vacuolar-type H⁺-translocating ATPase (v-ATPase) in follicular lymphoma (FL) highlights a role for the amino acid- and energy-sensing pathway to MTOR in the pathogenesis of this disease. Here, through the use of complementary experimental approaches involving mammalian cells and *Saccharomyces cerevisiae*, we have demonstrated that mutations in the v-ATPase subunit ATP6V1B2/Vma2 activate autophagic flux and maintain MTOR/Tor in an active state. Engineered lymphoma cell lines and primary follicular lymphoma B cells (FL B cells) carrying mutated ATP6V1B2 demonstrated a remarkable ability to survive low leucine concentrations. The treatment of primary FL B cells with inhibitors of autophagy uncovered an addiction for survival for FL B cells harboring ATP6V1B2 mutants. These data support mutational activation of autophagic flux by recurrent hotspot mutations in ATP6V1B2 as an adaptive mechanism in FL pathogenesis and as a new possible therapeutically targetable pathway.

Find the latest version:

<https://jci.me/98288/pdf>



Follicular lymphoma-associated mutations in vacuolar ATPase ATP6V1B2 activate autophagic flux and MTOR

Fangyang Wang^{1*}, Damián Gatica^{2,3*}, Zhang Xiao Ying¹, Luke F. Peterson¹, Peter Kim¹, Denzil Bernard¹, Kamlai Saiya-Cork¹, Shaomeng Wang¹, Mark S. Kaminski¹, Alfred E. Chang⁴, Tycel Phillips¹, Daniel J. Klionsky^{2,3*} and Sami N. Malek^{1,5*}

From the Department of Internal Medicine, Division of Hematology and Oncology¹, Life Sciences Institute², Department of Molecular, Cellular and Developmental Biology³, Department of Surgery⁴, University of Michigan, Ann Arbor, MI, USA.

Keywords: Follicular lymphoma, ATP6V1B2 mutations, autophagy, MTOR

Total Word Count: 11,638

*These authors contributed equally to this work.

⁵Correspondence should be addressed to: Sami N. Malek, Professor, Department of Internal Medicine, Division of Hematology and Oncology, University of Michigan, 1500 E. Medical Center Drive, Ann Arbor, MI 48109-0936. smalek@med.umich.edu. Phone: 734-763-2194. Fax: 734-647-9654.

Conflict of Interest

None to declare

Abstract

The discovery of recurrent mutations in subunits of the vacuolar-type H⁺-translocating ATPase (v-ATPase) in follicular lymphoma (FL) highlights a role for the amino acid- and energy-sensing pathway to MTOR in the pathogenesis of this disease. Here, through the use of complementary experimental approaches involving mammalian cells and *Saccharomyces cerevisiae*, we have demonstrated that mutations in the v-ATPase subunit ATP6V1B2/Vma2 activate autophagic flux and maintain MTOR/Tor in an active state. Engineered lymphoma cell lines and primary follicular lymphoma B cells (FL B cells) carrying mutated ATP6V1B2 demonstrated a remarkable ability to survive low leucine concentrations. The treatment of primary FL B cells with inhibitors of autophagy uncovered an addiction for survival for FL B cells harboring ATP6V1B2 mutants. These data support mutational activation of autophagic flux by recurrent hotspot mutations in ATP6V1B2 as an adaptive mechanism in FL pathogenesis and as a new possible therapeutically targetable pathway.

Introduction

Follicular lymphoma (FL) constitutes the most common indolent B-cell lymphoma, with an incidence and prevalence of ~14,000 and ~100,000 cases, respectively, in the US (1). FL remains incurable with conventional therapies and most patients receive multiple treatment regimens during the course of their illness. The development of targeted FL-directed therapies is in early stages (2-8) and the identification of novel targets remains a research priority.

An expanding group of recurrently mutated genes has recently been shown to underlie the pathogenesis of FL (*KMT2D/MLL2*, *CREBBP*, *TNFRSF14*, *EZH2*, *EP300*, *ARID1A*, *HIST1H1B-HIST1HE*, *STAT6*, *BTK*, *RRAGC*, those encoding components of the v-ATPase and others) and some of these may afford novel opportunities for targeted therapy developments (9-23). The rational design of such targeted therapies necessitates an in-depth understanding of the effects of mutations on the gene product, and the consequences for cellular function.

The identification of MTOR-activating mutations in the small G-protein *RRAGC*, a component of the amino acid signaling pathway to MTOR, has highlighted a potential opportunity to target this pathway in FL (24-26). Upstream of *RRAGC* in this pathway lays the multi-subunit vacuolar-type H⁺-translocating ATPase (v-ATPase) (27-29), which has also been identified as a commonly mutated target in FL (18, 24, 30). However, a comprehensive functional analysis of the consequences of point mutations in the various v-ATPase subunits has not been reported, and it remains unclear why FL among all B-cell non-Hodgkin's lymphoma would uniquely select for such mutations.

In this study, we examined the effect of mutations in the *ATP6V1B2* subunit of the v-ATPase on mammalian cell physiology. In addition, we took advantage of the conserved nature of the v-ATPase and generated a similar mutation in the yeast *VMA2* gene (31), allowing us to carry out certain assays that are not available in more complex eukaryotes. Together, the results indicate that the mutant *ATP6V1B2/Vma2* subunits result in compromised v-ATPase activity, causing an upregulation of macroautophagy/autophagy and autophagic flux. Even though there is an increase in autophagy, these

cells continue to display activity for MTOR/TOR, a major negative regulator of autophagy. These novel data suggest that it is possible to uncouple the amino acid status of the cell (which is affected by autophagy, and which regulates MTOR) and MTOR-dependent control of autophagy. In support of the physiological relevance of these novel findings, we show that one of the consequences of mutations in ATP6V1B2 is the ability of lymphoma cells to grow and survive under reduced leucine concentrations. This acquired ability to survive under nutrient stress is likely involved in the outgrowth of mutated FL cells and suggests opportunities for therapeutic interventions. Supporting the potential for such interventions, we demonstrated preferential sensitivity of ATP6V1B2 mutant primary FL B cells to inhibition of autophagic flux. In summary, our data provide novel insights into the role of macroautophagy and mutations in the v-ATPase in the pathogenesis of follicular lymphoma.

Results

The spectrum of *ATP6V1B2* mutations in 144 follicular lymphomas and 14 transformed follicular lymphomas

Recent reports of relatively frequent mutations in the v-ATPase subunit *ATP6V1B2* in follicular lymphoma and MTOR-activating mutations in *RRAGC*, along with reports of involvement of both proteins in a lysosomal amino acid-sensing pathway to MTOR, prompted us to study the underlying biology of these mutations (18, 24, 25, 27, 30). We first determined the frequency and nature of *ATP6V1B2* mutations in 144 FL and 14 transformed-FL (t-FL) using direct Sanger sequencing. We identified a total of 10% (16/158) of cases with non-synonymous *ATP6V1B2* mutations; of these, 3 *ATP6V1B2* mutations occurred in t-FL cases. The most common mutations in *ATP6V1B2* were located in the previously reported amino acid hotspots p.Y371Y>Y/C (N=5) and p.R400R>R/Q (N=8). In addition we detected the novel mutations p.D367E>D/E, p.R400R>RW and p.R471R>R/S (**Figure 1A**).

We found that clonal mutations in *RRAGC* and *ATP6V1B2* in FL did not occur together, suggesting that the corresponding proteins have overlapping functions in a shared pathway (see below) (24, 25).

FL-associated mutations in *ATP6V1B2* are located at the dimer interface with *ATP6V1A*

We modeled the location of the *ATP6V1B2* hotspot mutations p.Y371Y>Y/C and p.R400R>R/Q onto the published cryo-electron microscopy model of the yeast v-ATPase (32) (human *ATP6V1B2* protein has 77% sequence identity to its yeast counterpart). We found that both *ATP6V1B2* hotspot mutations are located at the interface of the two subunits that correspond to human/yeast v-ATPase subunits *ATP6V1A/Vma1* and *ATP6V1B2/Vma2* (**Figure 1B**). Zhao et al recently reported that the v-ATPase in yeast exists in three states (open, loose and tight) and that these states are linked to enzymatic activity, ATP/ADP binding and signaling to the *Vma3* subunit for proton translocation into the

organelle lumen (32). The three conformations are thought to bind ATP, ADP and phosphate, and no nucleotide, respectively. We found that yeast Vma2 residues Y352 and R381 (homologous to the FL-associated ATP6V1B2 hotspot mutations p.Y371Y>Y/C and p.R400R>R/Q), undergo significant conformational changes from one catalytic conformation to the other (**Supplementary Figure 1**) coupled with changes in the interaction with the partner Vma1. This suggests that the Y371C and R400Q mutations may have an impact on the interconversion between the 3 conformational states, influencing the rate and efficiency of the ATPase and proton pumping activity (33).

FL-associated ATP6V1B2 mutations activate autophagic flux

The v-ATPase is a key component of the cellular autophagic apparatus (34, 35); upon assembly on lysosomal membranes, it pumps protons into the lysosomal lumen, and the resulting acidification activates luminal proteases and peptidases, thus facilitating degradation of autophagy-derived and endocytic contents into free amino acids (36, 37). The proton gradient is also implicated in the inside-out active transport of amino acids from the lysosomal lumen into the cytoplasm as well as the activation of MTORC1 (27, 38).

We tested for possible effects of ATP6V1B2 mutations on autophagy using the steady state levels of the well-studied autophagosomal marker LC3-II (39). Nascent LC3 is typically cleaved at the C terminus, then conjugated to phosphatidylethanolamine (PE; termed LC3-II), allowing it to become associated with the membrane of the phagophore, and part of the LC3-II pool remains associated with the completed autophagosome.

Following transient transfection of HEK293T cells with either vector alone or vector containing cDNAs for wild-type or mutant HA-tagged ATP6V1B2 we detected highly elevated LC3-II levels in the mutant transfectants (**Figure 2A**). The LC3-II that remains associated with the autophagosome is located inside this compartment; subsequent fusion with the lysosome results in the degradation of this protein along with the autophagic cargo. For this reason, an increase in LC3-II may correspond to an

induction of autophagy, or to a block in the turnover of this protein in the lysosome (40). In order to distinguish between these two possibilities, we blocked lysosomal LC3-II degradation using the peptidase/hydrolase inhibitors pepstatin A and E-64D in parallel experiments, and detected a further increase in LC3-II levels (**Figure 2A,C**) indicative of elevated autophagic flux and normal fusion of autophagosomes with lysosomes in the mutant cells.

We generated various stable doxycycline-inducible lymphoma cell lines expressing wild-type (WT) or mutant ATP6V1B2 and conducted similar experiments to the above-detailed HEK293T cell experiments. Upon doxycycline induction of the expression of ATP6V1B2 in OCI-LY1 cells, we again detected highly elevated LC3-II levels in the mutants. Similar to the findings with HEK293T cells, treatment with pepstatin A and E-64D resulted in an additional increase in the levels of LC3-II (**Figure 2B,C**).

We also performed similar experiments with the v-ATPase inhibitor bafilomycin A₁ and found that LC3-II levels accumulated to higher levels than in the ATP6V1B2 mutants without inhibitor treatment (**Figure 2D-F**).

Next, we followed the protein levels of SQSTM1/p62 for 12 and 24 h after induction of wild-type and mutant ATP6V1B2 proteins (41). As can be seen in **Figure 2G-H**, SQSTM1 levels declined in the ATP6V1B2 mutants, in agreement with induction of autophagic flux.

To further investigate the effect of the ATP6V1B2^{R400Q} mutation on autophagy and autophagic flux we proceeded to test its effects in a yeast model. Sequence alignment showed that the ATP6V1B2^{R400Q} mutation corresponds to yeast Vma2^{R381Q}, and we generated a Vma2^{R381Q}-HA mutation in the genome. As a readout of autophagy activity, we measured GFP-Atg8 processing. Autophagy activation leads to the lipidation of Atg8 (akin to LC3-II in mammalian cells), which in turns leads to Atg8 binding to both sides of the phagophore. A portion of Atg8, or GFP-tagged Atg8, is delivered to the vacuole via autophagy; GFP is relatively resistant to vacuolar hydrolases and the free form can be resolved and detected by western blot. Accordingly, this assay directly monitors the

delivery of the autophagosome to the vacuole. The *Vma2*^{R381Q} mutant showed increased delivery of GFP-Atg8 and subsequent processing under both growing and nitrogen-starvation conditions indicative of elevated autophagic flux (**Figure 2I**). Furthermore, the GFP-Atg8 chimera is under the control of the endogenous *ATG8* promoter; the *ATG8* gene is substantially upregulated following autophagy induction. The increase in the amount of full-length GFP-Atg8 seen in the *Vma2*^{R381Q} strain even at time zero is another indication of upregulated autophagy as a result of the v-ATPase mutation.

As a parallel method of monitoring autophagic induction, we examined the endogenous Atg8 protein through a lipidation assay. The attachment of the Atg8 C terminus to PE results in a faster electrophoretic mobility relative to non-lipidated Atg8 (42). The cells expressing *Vma2*^{R381Q} showed increased Atg8 lipidation under growing and nitrogen-starvation conditions (**Figure 2J**).

Finally, autophagy activity was measured using the quantitative Pho8Δ60 assay (43). In brief, Pho8Δ60 is an engineered form of the Pho8 phosphatase that can only be delivered to the vacuole (the yeast equivalent of lysosomes) non-selectively through autophagy. Subsequently, the Pho8Δ60 propeptide gets cleaved by vacuolar hydrolases activating its phosphatase activity. The *Vma2*^{R381Q} mutant showed a significant increase in autophagy activity under both growing and nitrogen-starvation conditions (**Figure 2K**), which, was dependent on Atg1; deletion of *ATG1* (the yeast homolog of *ULK1*) fully prevented the induction of autophagic flux by nitrogen starvation or *Vma2*^{R381Q} (**Figure 2K**). Furthermore, a similar increase in autophagy activity was observed during nitrogen starvation in a strain carrying both a WT and R381Q mutant version of the *VMA2* gene (*Vma2*-HA WT/R381Q), a situation aimed at mimicking the heterozygous mutations occurring in FL tumors (**Supplementary Figure 2A-B**). Together, these data show that the mutation R381Q in *Vma2* increases autophagy activity, similar to the result seen with mutant ATP6V1B2 in mammalian cells.

FL-associated ATP6V1B2 mutant proteins activate MTOR

MTOR is the major regulator of cellular metabolism and a negative regulator of autophagy (44)(45)(46). We hypothesized that mutations in the v-ATPase resulted in a reduced degradation of lysosomal proteins and reduced release of amino acids from the lysosome, which would reduce MTOR activity (47, 48); this prediction would fit with the increase in autophagy activity.

HEK293T cells have been extensively used in the functional characterization of components of the v-ATPase-Ragulator-RRAGA/B/C/D-MTOR pathway (27, 49)(50). In doxycycline-inducible stable HEK293T cells induced for 24, 48 or 72 h we followed expression of ATP6V1B2, LC3-II, total RPS6KB/S6K and phosphorylation at residue Thr389 over time. With prolonged ATP6V1B2 induction, we found substantially elevated LC3-II and increased RPS6KB/S6K phosphorylation indicative of elevated MTOR activity (**Figure 3A**). We conducted an extensive series of similar experiments in doxycycline-inducible stable lymphoma cells and detected equivalent changes (**Figure 3B-E**; note that the induced expression of ATP6V1B2 p.R400Q in some of the lines is lower than for wild-type ATP6V1B2 or the p.Y371C mutation). The induction of MTOR activity was not immediate after ATP6V1B2 induction but was delayed.

We also measured MTOR activity in the inducible HEK293T cell lines using various p-EIF4EBP1 epitopes as readouts (**Supplementary Figure 3A-D**), and by monitoring RPS6KB/S6K in primary purified FL B cells in fully supplemented medium carrying either wild-type (N=5) or mutant (N=4) *ATP6V1B2* (**Figure 3F-G**). Overall, the data again supported elevated MTOR activity in ATP6V1B2 mutant cells.

As above, we proceeded with complementary experiments in yeast. To determine the effect of the Vma2^{R381Q} mutation on TOR activity, phosphorylation levels of three TOR substrates, Atg13, Npr1, and Gln3 (51)(52)(53) were used as readouts (**Figure 3H-J**). TOR phosphorylates these proteins in nutrient-rich conditions; however, during nitrogen starvation TOR inactivation leads to dephosphorylation of these target proteins, which can be observed by a downward shift in their

apparent molecular weight. During growing conditions (time zero), Atg13, Npr1 and Gln3 showed increased TOR phosphorylation in the *Vma2*^{R381Q} cells as evidenced by decreased mobility compared to the wild type, indicating that TOR was hyperactive in the mutant strain (**Figure 3H-J**). After 30 min of nitrogen starvation all three substrates displayed increased mobility in extracts from the WT strain, corresponding to a decrease in TOR activity. In contrast, Atg13, Npr1 and Gln3 still showed increased phosphorylation levels in the *Vma2*^{R381Q} mutant. This finding suggests that TOR is partially non-responsive to nitrogen depletion in *Vma2*^{R381Q} mutant cells. Together, the findings in mammalian cells and yeast support an MTOR-activated phenotype for FL-associated ATP6V1B2 mutant proteins.

The activation of autophagic flux and intact SLC38A9 functions are necessary for MTOR activation by mutant ATP6V1B2

Next, we decided to investigate the molecular mechanism responsible for the increase in autophagy activity in the presence of active MTOR/TOR. Considering the central role of ULK1/Atg1 in autophagy initiation we measured previously identified regulatory MTOR- and AMPK-mediated phosphorylation events in ULK1 (MTOR: phospho [p]-757-ULK1; AMPK: p-317-ULK1) in ATP6V1B2 doxycycline-inducible HEK293T and LY1 lymphoma cells. As expected, glucose deprivation strongly increased p-317-ULK1, and leucine deprivation reduced p-757-ULK1; however, neither site was substantially influenced by mutant ATP6V1B2 (**Supplementary Figure 4A-B**).

Next, we examined the role of the stress-responsive transcription factor ATF4 (54). We found that ATF4 protein expression was elevated in doxycycline-inducible HEK293T and LY1 lymphoma cells expressing ATP6V1B2 p.R400Q and to a lesser degree by ATP6V1B2 p.Y371C, indicative of metabolic stress (**Supplementary Figure 5A-B**). We disrupted *ATF4* in stable ATP6V1B2 wild type or mutant inducible HEK293T cells using Crispr-Cas9 targeting. While leucine starvation strongly induced ATF4 expression in the parental cells, its expression was completely lost after *ATF4* disruption

(Supplementary Figure 6A). However, LC3-II levels remained highly elevated in the ATP6V1B2 mutant strains lacking ATF4, arguing against a critical role for this transcription factor in autophagic flux initiation by mutant ATP6V1B2 **(Supplementary Figure 6B).**

The yeast homolog of ATF4, Gcn4, has been implicated in autophagy regulation (55, 56). Accordingly, we measured the expression of several *ATG* genes in *S. cerevisiae* carrying Vma2 wild type or the Vma2^{R381Q}-HA knock-in point mutation (55, 56). Under full-medium culture conditions, we detected substantially elevated expression of these *ATG* genes in the cells carrying Vma2^{R381Q}-HA, further supporting the autophagy-inducing properties of the ATP6V1B2 mutants **(Supplementary Figure 6C).** Subsequently, we deleted *GCN4* or the gene encoding its upstream regulatory kinase, *GCN2* (EIF2A/eIF2 α kinase) in these yeast strains. Despite the deletion of one or both of these genes, the elevated expression of the *ATG* genes persisted—although there did appear to be a partial reduction in the double-knockout strain—arguing against the Gcn2-Gcn4 pathway as the critical mediator of autophagy induction in the ATP6V1B2 mutants **(Supplementary Figure 6C).**

The second major phenotype resulting from the ATP6V1B2/Vma2 point mutations was the delayed activation of MTOR/TOR under nutrient-stress (i.e., normally inactivating) conditions. To understand the relationship between activation of autophagic flux and MTOR activation we generated HEK293T cells null for *ATG7*, a critical component of the autophagic machinery. Clonal HEK293T *ATG7*^{-/-} cells that also carried inducible wild-type and mutant ATP6V1B2 expression cassettes were generated, and expression of ATP6V1B2 proteins induced using doxycycline. While the induction of LC3-II and MTOR activation was readily detectable in the *ATG7* wild-type cells that had also gone through the CRISPR-Cas9 targeting process, both phenotypes were abolished in the *ATG7*^{-/-} cells **(Figure 4A-B).** This finding indicates that the activation of autophagic flux is the primary molecular consequence of mutations in ATP6V1B2, and that intact macroautophagy is required for the observed delayed MTOR activation.

The previously reported delayed reactivation of MTOR following starvation has been ascribed to the substantial upregulation of autophagic flux under starvation conditions (57). We reasoned that increased cargo delivery to lysosomes would activate MTOR through canonical pathways and mechanisms. Given the recently elucidated role of SLC38A9 in amino acid sensing and transport in lysosomes we proceeded to generate HEK293T SLC38A9^{-/-} cells (58-60). While the induction of LC3-II and MTOR was readily detectable in the SLC38A9 wild-type cells that had also gone through the CRISPR-Cas9 targeting process as expected, both phenotypes were abolished in the SLC38A9^{-/-} cells (**Figure 4C-D**). Combined, the data strongly suggest that increased protein delivery to lysosomes followed by elevated lysosomal amino acid concentrations and signaling through SLC38A9 ultimately results in MTOR activation in the setting of aberrantly persistent elevated autophagic flux conditions.

Mutant ATP6V1B2 confers a defect on the v-ATPase holoenzyme proton pump

Given the central role of the v-ATPase as a proton pump, we proceeded with measurements of lysosomal pH in stable transduced HEK293T cells expressing WT or mutant ATP6V1B2. Cells were loaded with a pH-sensitive dual reporter dye conjugated to dextran and the cells were subsequently analyzed using a fluorescence-activated cell sorter. As controls, cells in parallel were briefly incubated with buffers at a defined pH of 3.5, 4.5 or 5.5, respectively (**Figure 5A upper row**), or were treated with bafilomycin A₁ to completely inhibit v-ATPase function (**Figure 5A; lower row**). Whereas treatment with bafilomycin A₁ resulted in an elevated pH in all cells as expected from its ability to completely inhibit the v-ATPase, we detected an acidic lysosomal pH in the range of 4.5 for the ATP6V1B2 wild-type and an acidic lysosomal pH in the range of >4.5 – 5.5 in the mutant cell lines; therefore, the mutants displayed a reduced ability for acidification (**Figure 5A; middle row**).

We extended this analysis to determine if the R381Q mutation in Vma2 affects the ability of the V-ATPase to acidify the vacuolar lumen in yeast. To this end, the Pho8 C terminus was tagged with a pH-sensitive Super Ecliptic pHluorin (SEP) protein that displays increased fluorescence with increased

pH (61). Similar to the control *vma2Δ* strain, *Vma2*^{R381Q} cells showed increased vacuolar pH compared to WT cells (**Figure 5B-C**) (33).

Increased lysosomal localization of mutant ATP6V1B2 proteins and increased interaction with the LAMTOR (Ragulator) complex

The v-ATPase is composed of two primary subcomplexes, which can associate and dissociate in response to changing nutrient conditions (62) (63). We tested if the two hotspot mutations in ATP6V1B2 (**Figure 1B**) affected interaction with ATP6V1A and therefore could have effects on the assembly of an intact v-ATPase. In transient co-transfection studies in HEK293T cells expressing HA-tagged WT and mutant ATP6V1B2 followed by HA-bead-based immunoprecipitations, we detected no effect of the ATP6V1B2 mutants on the amount of co-immunoprecipitated ATP6V1A (**Supplementary Figure 7**).

Next, we assessed the amount of WT and mutant ATP6V1B2 localizing to lysosomes using confocal microscopy. Using fluorescence color changes as a readout for colocalization of ATP6V1B2 and LAMP1 (an endosomal and lysosomal membrane marker), we detected increased amounts of mutant ATP6V1B2 on endosomes and/or lysosomes when compared with the WT ATP6V1B2 staining (**Supplementary Figure 8A-B**).

To study the interaction between ATP6B1V2 and the LAMTOR proteins (49), we transiently co-transfected plasmids encoding HA-tagged WT or mutant ATP6V1B2 together with a mixture of plasmids that express FLAG-tagged LAMTOR1-LAMTOR5 into HEK293T cells. After cell lysis we performed reciprocal co-IPs using anti-HA- or anti-FLAG-conjugated beads. Upon immunoblotting of lysates and immunoprecipitates, we detected modestly increased interaction of the mutant ATP6V1B2 protein (anti-HA band) with the LAMTOR complex (compare lane 2 with lanes 3 and 4) (**Supplementary Figure 8C**).

Improved survival and growth of lymphoma cell lines carrying mutant *ATP6V1B2* cultured under leucine-deprivation conditions

We hypothesized that the dual activation of autophagic flux and MTOR by the FL-associated *ATP6V1B2* mutant proteins may confer increased survival or pro-growth properties on afflicted lymphoma cells. To test this hypothesis, we used lentivirus-based transient dual sequential transductions of *ATP6V1B2* wild type and mutants into the SUDHL4 lymphoma cell line, and 48 h later we incubated cells in full medium (100% leucine [Leu]) or in medium with only 25% Leu. We followed cell counts and viability for nine days post infection. For the cells grown in full medium we noticed no significant differences; however, for the cells grown in 25% Leu we measured significantly more viable mutant cells. Data from 4 independent experiments are summarized in **Supplementary Figure 9A-B** indicating a survival or growth advantage especially for the cells carrying the *ATP6V1B2* R400Q mutation.

Next, we took advantage of the doxycycline-inducible stable cell lines described above. Similar to the experiments using SUDHL4 cells, we incubated cell lines expressing WT or mutant *ATP6V1B2* after doxycycline induction for 48 h in either full-or limited-leucine medium. Whereas OCI-LY1 cell lines carrying the *ATP6V1B2* mutants grew less well under full-medium conditions (**Supplementary Figure 9C**), both lines survived substantially and significantly better in low leucine (**Supplementary Figure 9D-F**).

Improved survival and growth of primary follicular lymphoma B cells carrying mutant *ATP6V1B2* cultured under leucine-deprivation conditions

Next, we studied primary human FL B cells purified from cryopreserved lymphoma biopsy specimens. FL B cells carrying WT (N=5) or mutant (N=6) *ATP6V1B2* were cultured in dialyzed serum-supplemented RPMI1640 medium containing either 100% Leu or various reduced Leu concentrations depending on the availability of sufficient cells. FL B cells were cultured and the cell number and fraction

of living cells was determined for up to 5 days. FL B cells carrying WT *ATP6V1B2* demonstrated substantial cell death induction in the first 24-48 h of culture under reduced Leu concentrations (**Figure 6A**); in contrast, most FL B cells carrying mutated *ATP6V1B2* largely survived under low Leu (**Figure 6B**); at all tested Leu concentrations, a substantially larger fraction of FL B cells carrying mutated *ATP6V1B2* survived (**Figure 6C-D**). Even at 0% Leu, greater than 60% of FL B cells carrying mutated *ATP6V1B2* survived while only ~20% of cells carrying wild-type *ATP6V1B2* remained alive.

These data support the hypothesis that FL-associated *ATP6V1B2* mutations facilitate lymphoma cell growth and survival under conditions of amino acid deprivation likely through generation of free leucine resulting from elevated autophagy.

Primary human follicular lymphoma B cells carrying mutant *ATP6V1B2* are sensitive to inhibition of autophagic flux

In preliminary experiments we incubated purified FL B cells in fully supplemented RPMI1640 medium and added the autophagy inhibitor bafilomycin A₁ (35). We determined the cell fractions alive or apoptotic/dead using ANXA5/annexinV-propidium iodide-based flow analyses. We found that FL B cells from 4 out of 5 cases carrying mutated *ATP6V1B2* demonstrated sensitivity to bafilomycin A₁, whereas only 1 out of 5 cases carrying wild-type *ATP6V1B2* demonstrated sensitivity (**Supplementary Figure 10**). These data provided preliminary evidence that autophagic flux sustains survival of the *ATP6V1B2*-mutated FL B cells.

Two recent reports describe the discovery and functional studies of novel ULK1 kinase inhibitors (MRT68921 and SBI-0206965) (64, 65). We confirmed the ability of both molecules to inhibit the phosphorylation of the direct ULK1 substrate ATG13 (**Supplementary Figure 11**) and based on potency selected MRT68921 for further studies. We treated primary purified human FL B cells isolated from lymph node biopsies that carried wild-type or mutant *ATP6V1B2* with escalating doses of MRT68921 and measured the cell fraction alive after 48 h using ANXA5/annexinV-propidium iodide-

based flow analyses. We found that FL B cells carrying mutant ATP6V1B2 were substantially and significantly more sensitive to ULK1 inhibitor-induced cell death than ATPV1B2 wild-type lymphoma cells (**Figure 7 A-B**).

We also tested the ULK1 inhibitor MRT68921 in combination with MTOR inhibitors (rapamycin or torin 1) or chemotherapeutics (doxorubicin or vincristine) used clinically to treat FL patients (**Supplementary Figure 12A-H**). We found that ULK1 and MTOR inhibition was antagonistic, which is likely the result of MTOR inhibitor-mediated further elevations in autophagic flux (**Supplementary Figure 12E-F**). In contrast, the combinations of ULK1 inhibitors with doxorubicin and especially with vincristine preferentially enhanced the killing of ATP6V1B2 mutant FL B cells and in this context it is of interest that vinblastine, a drug with properties similar to vincristine, is known to inhibit autophagic flux (**Supplementary Figure 12G-H**) (66).

In summary, these data uncover a survival addiction to activated autophagic flux in ATP6V1B2 mutant FL B cells, which we posit offers opportunities for novel therapeutic approaches in FL.

Discussion

Whole exome sequencing has begun to provide directions for investigating the genetic basis of follicular lymphoma (11-13, 15, 18, 30). For example, recurrent mutations in RRAGC and subunits of the v-ATPase in FL suggest a role for amino acid (via the RRAG proteins) and energy sensing (through the v-ATPase) mechanisms that feed into the regulation of MTOR in the pathogenesis of follicular lymphoma. Whereas mutations in RRAGC activate MTOR in part through facilitated interactions with RPTOR (24, 25), the functional consequences of mutations in the v-ATPase subunits remained unexplored. FL-associated mutations in the v-ATPase occur predominantly in *ATP6AP1* and *ATP6V1B2*, the latter a principle component of the multimeric V₁ hexameric subunit of the v-ATPase.

In this study, we set out to address the mechanistic consequences of the heterozygous *ATP6V1B2* hotspot mutations p.Y371Y>Y/C and p.R400R>R/Q, which occur at a frequency of 10% in FL. Given the established roles of v-ATPase as a major component of the autophagy machinery important for acidification of lysosomes and its role in regulating MTOR through mechanisms that remain not fully defined, we focused our initial studies on these pathways. Through a series of complementary experiments in mammalian cells as well as in *S. cerevisiae* we made the following novel observations: i) the *ATP6V1B2* hotspot mutations activate autophagy and autophagic flux; ii) the *ATP6V1B2* hotspot mutations also activate MTOR, identifying for the first time a gene mutation activating both pathways simultaneously; iii) lymphoma cell lines and primary FL B lymphoma cells harboring *ATP6V1B2* hotspot mutations survive and/or grow better in media containing lowered concentration of the amino acid leucine, demonstrating that these mutations counteract the effects of nutrient deprivation, and providing a credible pathophysiological selective advantage conferred by these mutations; and, iv) FL B cells harboring mutant *ATP6V1B2* are dependent on autophagic flux for survival.

The lysosomal acidification caused by activated v-ATPase enables activation of a set of lysosomal-resident peptidases that facilitate degradation of proteins delivered to the lysosome.

Previous work has demonstrated that autophagosome-lysosome fusion can proceed in the absence of v-ATPase but the resulting neutral lysosomal pH is unlikely to support the generation of sufficient free amino acids for active cell growth (35). We find in mammalian cells and yeast that mutated ATP6V1B2/Vma2 is hypomorphic and results in modestly impaired lysosomal acidification. Simultaneously, the amount of lysosomal v-ATPase is increased suggesting a compensatory adaptation. In addition, the impaired lysosomal acidification is associated with a substantial increase in autophagic flux suggesting again a compensatory adaptive mechanism. The substantial increase in autophagic flux constitutes one principle mechanism of FL-associated mutations in ATP6V1B2. These findings, combined with a recent report demonstrating an inhibitory role of EP300 on autophagy through PIK3C3/VPS34 acetylation and the frequent genetic inactivation of EP300 in FL, suggest that mutational activation of autophagy is prevalent in FL (13, 67).

Somewhat unexpectedly, we measured increased MTOR activity in recombinant lymphoma cells, primary FL B cells and towards various protein substrates in yeast. The activation of MTOR in lymphoma cells carrying inducible ATP6V1B2 transgenes was delayed, compatible with a model in which activation of autophagic flux precedes, and ultimately results in, the activation of MTOR. In support of this model, ablation of autophagic flux through ATG7 inactivation prevented ATP6V1B2 mutants from activating MTOR. Given the previous findings of an inside-out signaling pathway (lysosomal lumen to cytoplasm) for amino acids leading to MTOR activation (27) (68), we generated *SLC38A9* knockout cells and confirmed the essential role for this amino acid sensor/transporter in MTOR activation by mutant ATP6V1B2.

In the course of these studies we show for the first time an effect of ATP6V1B2 mutations on the survival or growth of lymphoma cell lines and primary FL B cells under experimentally lowered leucine concentrations. These data fully support the hypothesis that lymphoma cells carrying ATP6V1B2 mutations are preferentially able to generate leucine from internal stores, likely through the activation of autophagy. This interpretation is furthermore supported by the fact that the majority of primary FL B

cells carrying ATP6V1B2 mutations are preferentially sensitive to autophagy inhibitors. The latter findings may open up novel avenues for the treatment of FL, possibly through intermittent inhibition of autophagy (69, 70), and inhibitors of ULK or VPS34 kinases that are in development may be useful in this setting (64, 65) (71).

In summary, our studies elucidate novel mechanisms of action of FL-associated mutations in components of the v-ATPase demonstrating for the first time dual activation of autophagy and MTOR, and provide a framework for future biological or therapeutic studies of v-ATPase in follicular lymphoma.

Methods

Patient characteristics and study source material

Results from the Sanger-based resequencing of *ATP6V1B2* using template DNA isolated from 144 flow-sorted FL and 14 flow-sorted t-FL are reported here. Methods for fluorescence-activated cell sorting (FACS) of lymphoma specimens are as described previously (12). Eighty-five FL and 14 t-FL patients (cohort I) were enrolled in two separate lymphoma repositories at the University of Michigan. We furthermore analyzed by Sanger sequencing DNA from 59 sorted FL cases (cohort II) collected between 1990 and 2005 as previously described that were derived from de-identified leftover clinical material (72).

Exon resequencing of *ATP6V1B2* in FL

Primers were designed to amplify and sequence all coding exons and adjacent intronic sequences of *ATP6V1B2* using direct sequencing as described (12). Mutations were confirmed to be somatically acquired using unamplified follicular lymphoma cell-derived DNA and paired CD3 cell-derived DNA as templates isolated from flow-sorted cells.

ATP6V1B2 cDNA mutagenesis, retroviral and lentiviral vector generation, cell transfection and cell transduction to generate stable cell lines.

Cell lines: The OCI-LY1 line was obtained from the Ontario Cancer Institute, Toronto, Canada. The SUDHL4 cell line was obtained from Dr. Elenitoba-Johnson (University of Michigan, Ann Arbor). Cell line authentication was performed through sequence analysis of six to eight gene mutations per line based on the COSMIC cell line project (catalogue of somatic mutations in cancer; http://cancer.sanger.ac.uk/cell_lines). The SUDHL16 cell line was purchased from the DSMZ repository (<https://www.dsmz.de/>).

Reagents and mutagenesis: A plasmid containing the *ATP6V1B2* cDNA (CH817565) was purchased from Vigene, and used as a template to generate mutant *ATP6V1B2* cDNAs using the QuikChange® Lightning Site-Directed Mutagenesis Kit (Stratagene/Agilent, La Jolla, CA). Full-length wild-type and mutant HA-tagged *ATP6V1B2* were constructed using PCR and cloned into the lentiviral FG9 vector (a gift from Dr. Colin Duckett, Ann Arbor, MI) (73) or into the retroviral vector MSCV-IRES-PURO (MIP) (74). Full-length WT and mutant HA-tagged *ATP6V1B2* were subcloned into the doxycycline-inducible plasmid pCW57.1 (Addgene, #41393; deposited by Dr. David Root) using Gateway cloning (Life Technologies).

Transient transfection studies in HEK293T cells: HEK293T cells were transfected in 10-cm dishes with 3 µg of MIP plasmids encoding either WT or mutant forms of *ATP6V1B2* or various other constructs as indicated using polyethylenimine (PEI; Polyscience Inc., #23966).

Generation of stable transduced HEK293T cell lines: HEK293T packaging cells were transfected with 5 µg of lentiviral vector (either the vector alone or vector expressing WT or various mutant forms of HA-*ATP6V1B2*), together with 1 µg of the plasmids REV, RRE and VSVG. Viral supernatant media were collected 48-72 h after transfection and cleared by low-speed centrifugation to remove cells and debris.

SUDHL4 cells were double spin-inoculated at 30°C at 2600 rpm using 8 µg/ml of polybrene for 2 h on day 0 and day 1 with recombinant FG9 lentiviruses carrying WT or mutant cDNAs encoding HA-*ATP6V1B2*. The infection efficiency was confirmed on day 3 through FACS based on GFP fluorescence and was >90%. Cells were sorted on GFP high fluorescence.

Generation of stable doxycycline-inducible lymphoma cell lines: The lentiviral expression vector pCW57.1 was used to generate stable doxycycline-inducible cell lines of OCI-LY1, SUDHL4, and SUDHL16. After viral transduction, cells were treated with 2 µg/ml of puromycin for 3-5 days and dead cells removed using Histopaque-1077 gradient centrifugation (Sigma-Aldrich, RNBFB2746), and subsequently cultured in regular medium; cultured pools were used for experiments described herein.

The inducible expression of ATP6V1B2 following doxycycline treatment (1,000 ng/ml for 24-72 h) was verified by immunoblotting for ATP6V1B2 and HA.

Generation of stable doxycycline-inducible HEK293T cell lines: Stable doxycycline-inducible HEK293T cell lines carrying WT or mutated *HA-ATP6V1B2* cDNAs were generated using the pCW57.1 vector as outlined above. The inducible expression of ATP6V1B2 following doxycycline treatment (1,000 ng/ml for 24-72 h) was verified by immunoblotting for ATP6V1B2 and HA.

Culture and survival analyses of various stable cell lines in full medium and during leucine deprivation

All experiments were performed at ambient O₂ levels and 5% CO₂. Prior to leucine starvation, SUDHL4 and SUDHL16 cells were cultured in RPMI1640 medium supplemented with 10% FCS. OCI-LY1 cells were cultured in DMEM supplemented with 20% fetal bovine serum (FBS) and 50 μM beta-mercaptoethanol. To control for the leucine concentration, we used leucine-free RPMI medium (Sigma-Aldrich, R1780; with re-added Arg and Lys), leucine-free DMEM medium (Sigma-Aldrich, D9443; with re-added Arg and Lys) and dialyzed FCS using dialysis tubing (Sigma-Aldrich, D7884).

Stable SUDHL4 cells expressing WT or mutated ATP6V1B2 were seeded at 5X10⁵ cells per ml and cultured in full RPMI 1640 medium supplemented with 20% FBS. Parallel cell aliquots were cultured under otherwise identical conditions but using only 25% of the leucine concentration.

Doxycycline-inducible stable OCI-LY1 or SUDHL16 cell lines were induced with 1,000 ng/ml doxycycline on day 0 and after 48 h (day 2); cells were seeded at 5x10⁵ cells per ml and cultured in full DMEM or RPMI medium supplemented with 10% FBS. Parallel cell aliquots were cultured under otherwise identical conditions but using reduced leucine concentrations as indicated. Cells were counted every other day using Trypan blue staining and diluted back to a concentration of 5x10⁵ cells per ml.

MTOR signaling and autophagy assays in inducible stable cell lines

Doxycycline-inducible stable OCI-LY1, SUDHL4 or SUDHL16 cell lines were induced with 1,000 ng/ml doxycycline for 24, 48, or 72 h. Cells were seeded at 5×10^5 cells per ml and cultured in full DMEM or RPMI medium supplemented with 10% FBS. The cell pellets were lysed in lysis buffer containing 1% NP-40, 150 mmol/L NaCl, 25 mmol/L Tris, pH 8.0, 20 mmol/L NaF, 2 mmol/L EGTA, 2 mmol/L EDTA, supplemented with protease inhibitors (Sigma-Aldrich, P3840), phosphatase inhibitors (Sigma-Aldrich, P0044), sodium orthovanadate (Sigma-Aldrich, 450243) and PMSF (Thermo Scientific, 36978). The detergent-soluble fraction of cell lysates was cleared by centrifugation at 14,000 rpm for 10 min. Protein was fractionated through SDS-PAGE and prepared for immunoblotting using standard procedures. For analyses of autophagic flux, various cell lines as indicated below were treated with the v-ATPase inhibitor bafilomycin A₁ at 100 nM for 4 h or with the protease (hydrolase) inhibitors pepstatin A for 12 h at 100 µg/ml and E-64d for 1 h at 10 µg/ml. Cells were harvested and prepared for immunoblotting with various antibodies as indicated (Supplemental Table 1). Band intensities were analyzed by densitometry (ImageJ2, v2.0.0).

Generation of HEK293T cells lacking intact *ATG7* or *SLC38A9*

We generated HEK293T *ATG7*^{-/-} or *SLC38A9*^{-/-} cells using pLENTIcrispr v2 (75) containing guides with the following sequences: *ATG7*, sense: GAAGCTGAACGAGTATCGGC; antisense: CACCGGAAGCTGAACGAGTATCGGC and *SLC38A9*, sense: AACTGGATATTCATAGGTCC; antisense: GGACCTATGAATATCCAGTT. After lentiviral infection, single-cell cloning and screening of clones by immunoblotting, two independent single-cell clones for *ATG7* or *SLC38A9* were selected for further study. As controls, we employed single cell clones that had gone through the entire gene targeting process but remained *ATG7* or *SLC38A9* wild type. To generate stable doxycycline-inducible ATP6V1B2-overexpressing cells, we infected all single-cell clones (*ATG7*^{-/-} or *SLC38A9*^{-/-} and controls)

with the doxycycline-inducible recombinant lentiviral pCW57.1 vectors followed by puromycin selection as outlined above.

ATF4 expression and ULK phosphorylation assays in ATP6V1B2-inducible stable cell lines

Doxycycline-inducible stable HEK293T or OCI-LY1 cell lines carrying wild-type or mutant ATP6V1B2 were induced with 1 µg/ml of doxycycline for 48 h and incubated in fresh doxycycline-free medium for 4 h prior to harvesting. Stable HEK293T or OCI-LY1 cells carrying empty vector were incubated in full medium, glucose-free medium or leucine-free medium, respectively for 4 h as controls. Western blotting was used to detect ATF4 expression and ULK phosphorylation.

Measurement of lysosomal pH in stable transfected HEK293T cells

HEK293T cells overexpressing WT or mutated HA-ATP6V1B2 were grown in 24-well plates. LysoSensor Yellow/Blue dextran (500 µg/mL; ThermoFisher Scientific, L22460) was added and cells incubated for 16 h, followed by a 1-h chase in dextran/dye-free medium. Subsequently, cells were trypsinized and washed, and cell samples immediately analyzed by flow cytometry. The wavelength of the fluorescence emitted by LysoSensor Yellow/Blue dextran is pH dependent; in an acidic environment, LysoSensor Yellow/Blue dextran emits in the yellow spectrum and in a neutral or basic environment, emission is in the UV spectrum. We measured fluorescence emitted at 405 and 526 nm in response to excitation at 355 and 448 nm, respectively, and subtracted the signal from unstained cells (background fluorescence control). Parallel cell samples for pH calibration were generated using fluorescein-dextran-loaded cells and a 25 mM MES calibration buffer (adjusted to a pH of 3.5–6.0 in 0.5 pH unit increments), containing 10 µM monensin, 10 µM nigericin, 5 mM NaCl, 115 mM KCl, and 1.2 mM MgSO₄.

Localization of wild-type and mutant HA-ATP6V1B2 in stable transfected HEK293T cells using confocal microscopy

Cells were plated on pre-sterilized cover slips. Cells were fixed and permeabilized with 4% paraformaldehyde for 10 min at room temperature and subsequently in 0.1% Triton X-100 for 5 min at 4°C. Samples were blocked with 4% bovine serum albumin (BSA) in phosphate-buffered saline (PBS) for 1 h at room temperature. Staining was performed using primary antibodies diluted in 4% BSA in PBS. Species-specific conjugated secondary antibodies (Supplemental Table 1) were diluted 1:1000 in 4% BSA in PBS and applied for 1 h at room temperature. Nuclei were counterstained with 4',6-diamidino-2-phenylindole (DAPI; Molecular Probes). The coverslips were mounted onto glass slides with ProLong Gold anti-fade reagent (Invitrogen, 1811419). Images were taken using a Leica SP5 confocal imaging system. Colocalization assays were performed using ImageJ v2.0.0 software.

Immunoprecipitation assays

Cells were pelleted, washed and lysed on ice for 20 min in lysis buffer containing 0.3% CHAPS detergent (Dot Scientific, DSC41010), 100 mM NaCl, 25 mM Tris, pH 8.0 (Sigma-Aldrich, T6066), 20 mM NAF, 2 mM EGTA, 2 mM EDTA (Sigma-Aldrich, ED2SS), supplemented with protease and phosphatase inhibitors, sodium orthovanadate, and PMSF. The detergent-soluble fraction of the cell lysates was cleared by centrifugation at 14,000 rpm for 10 min. For anti-HA or anti-FLAG immunoprecipitations, anti-HA-loaded beads (Sigma-Aldrich, A2095) or anti-FLAG-loaded beads (Sigma-Aldrich, A2220) were blocked with 5% BSA in TBST (25 mM Tris, pH 7.5, 150 mM NaCl, 0.05% Tween 20) for 0.5 h, then washed three times with lysis buffer. Next, 20 µl anti-HA or anti-FLAG-conjugated beads were added to pre-cleared cell lysates and incubated with rotation for 5 h at 4°C. The beads were washed 4 times with lysis buffer and protein was liberated through boiling in SDS-PAGE loading buffer. Protein was fractionated through SDS-PAGE and prepared for immunoblotting

using standard procedures. For immunoblottings, the detergent was 1% NP-40 instead of CHAPS (see immunoprecipitation conditions above) and NaCl was at 150 mM.

FL cell column purification through negative selection

Cryopreserved single-cell suspensions from human FL biopsy samples were thawed, washed and resuspended in degassed BSA-EDTA (1 X PBS, 0.5% BSA, 1 mmol/L EDTA) buffer at an approximate concentration of 10^7 cells per 60 μ l. Cells were treated with 20 μ l per 10^7 cells of Miltenyi CD3 magnetic microbeads (130050101) and 20 μ l per 10^7 cells of Miltenyi CD14 magnetic microbeads (130050201) and incubated at 4°C for 25 min. Cells were washed with BSA-EDTA, resuspended in 500 μ l of BSA-EDTA and passed through Miltenyi LS columns (145387) loaded onto a QuadriMax magnet as per the manufacturer's recommendations. The flow-through fraction containing CD3⁻ and CD14⁻ highly enriched FL B cells was centrifuged and resuspended in RPMI1640 medium supplemented with 20% heat inactivated FBS.

Drug treatment and apoptosis assays of FL cells

Purified FL cells were plated in RPMI1640 medium supplemented with 20% heat inactivated FBS at a density of 10^6 cells/ml and cultured at 37°C with 5% CO₂. MRT 68921 (1190379), bafilomycin A₁ (11038), rapamycin (13346), torin 1 (10997), doxorubicin (15007), dexamethasone (11015), vincristine (11764), and chloroquine (14194) procured from Cayman Chemicals were diluted serially in medium and DMSO-only was used as vehicle control. After 72 h of incubation, cell viability was measured with Celltiter-Glo® (Promega, G7572) and quantified on a Glomax® microplate reader (Promega, SA3030). For apoptosis readouts after 72 h of incubation, cells were washed twice with HBSS. The ANXA5/annexin V-FITC reagent (SouthernBiotech, 10039-02) was 1:20 diluted in ANXA5/annexin V-binding buffer (10 mmol/L HEPES, 140 mmol/L NaCl, 2.5 mmol/L CaCl₂, 0.1% BSA, pH7.4), added to each sample and incubated on ice in the dark for 15 min. Subsequently, 400 μ l of

ANXA5/annexin V-binding buffer and 20 μ l of 20 μ g/ml propidium iodide (PI) solution were added and samples immediately analyzed by flow cytometry.

Survival analyses of primary purified FL B cells in full medium and during leucine deprivation

Purified FL B cells were plated in RPMI1640 medium supplemented with 20% heat inactivated FBS at a density of 10^6 cells/ml. Parallel cell aliquots were cultured under otherwise identical conditions but using a reduced leucine concentration of 25, 12.5, 6.25 or 0%. Cells were counted and viability assessed on days 1, 2, 3 and 5 using Trypan blue staining.

Immunoblotting of lysates of cultured primary purified FL B cells

Purified FL cells were resuspended in RPMI1640 medium supplemented with 20% heat-inactivated FBS at a density of 10^6 cells/ml and cultured at 37°C with 5% CO₂ for 4 h. Cells were washed once, pelleted and rapidly frozen using dry ice thereafter. Cell pellets were lysed and prepared for immunoblotting as described above.

Computational methods

Several homology models of the ATP6V1B2 subunit were generated using servers on protein model portal, and structural alignment was performed using Pymol. Structures of the yeast v-ATPase were downloaded from the PDB (ID: 3J9T, 3J9U, and 3J9V), and aligned using residues Y352 and R381 in Pymol.

Yeast methods

Saccharomyces cerevisiae strain WLY176 was used to generate a VMA2-HA R381Q point mutation in the genome as previously described (76, 77). Deletion strains *gcn2 Δ* , *gcn4 Δ* and *gcn2 Δ gcn4 Δ* were also generated from WLY276 as previously described (78). The WLY176 VMA2-HA

WT/WT and WT/R381Q strains were generated by AflII digestion of a pRS405 plasmid containing either VMA2-HA WT or R381Q. The pRS405 VMA2-HA plasmid was constructed through fast cloning (79). Site-directed mutagenesis of pRS405 VMA2-HA was performed as previously described (80). Pho8 Δ 60 and GFP-Atg8 western blot analyses were performed as previously described (81) (82). A vacuolar fluorescence Pho8-SEP assay was developed according to a previous paper (61). For culture, yeast strains were grown in YPD medium (1% [w:v] yeast extract, 2% [w:v] peptone, and 2% [w:v] glucose) to mid-log phase and then collected. Strains grown in YPD were shifted into minus-nitrogen medium (0.17% yeast nitrogen base without ammonium sulfate or amino acids, and 2% [w:v] glucose) for the indicated time points and then collected. Fluorescence measurements were performed using ImageJ software. RNA extraction and qPCR experiments were performed as described previously (83).

Statistical Methods

Statistical comparisons were carried out using unpaired two-sample t-tests (for comparisons between two conditions), or linear regression (for tests involving more than two conditions). In the latter case, linear contrasts were constructed and tested against a null value as appropriate using standard regression-based Wald-type tests. For example, if measurements are made under mutant (mut) and wild-type (wt) cells in two environments A and B, the contrast "A:mut - A:wt - (B:mut - B:wt)" would be compared to zero to assess whether the impact of the mutation differs in the two environments. Regression models included blot fixed effects for all measurements obtained from the same blot. Bonferroni adjustments were used when a positive result from any one of several tests would be used to support a single hypothesis.

Study Approvals

The lymphoma repositories IRBMED #HUM00007985 and IRBMED #HUM00017055 were approved by the institutional review board (IRBMED) of the University of Michigan, Ann Arbor,

Michigan and all patients signed informed consent documents. Genomic research on all specimens was approved through IRBMED #HUM00005467 (Genomic analysis of B-cell non-Hodgkin's lymphoma).

AUTHOR CONTRIBUTIONS

Mark Kaminski, Alfred Chang, Tycel Phillips and Sami N. Malek enrolled patients and analyzed clinical data.

Fangyang Wang, Damián Gatica Mizala, Zhang Xiao Ying, Peter Kim, Luke F. Peterson, Kamlai Saiya Cork and Sami Malek performed the laboratory research.

Denzil Bernard and Shaomeng Wang assisted with the structural modeling.

Damián Gatica Mizala and Daniel Klionsky performed and/or interpreted all yeast experiments.

Sami Malek and Daniel J. Klionsky conceived the study and wrote the paper

ACKNOWLEDGEMENTS

We are grateful for services provided by the genomics and bioinformatics core of the University of Michigan Comprehensive Cancer Center. We are grateful to Dr. Kerby Shedden, Professor of Statistics, University of Michigan, Ann Arbor for consultations.

FUNDING SOURCES

This work was supported by R01CA190384 (to SNM), the Weatherhall foundation (to MK), and R01GM053396 (to DJK).

REFERENCES

1. Morton LM, Wang SS, Devesa SS, Hartge P, Weisenburger DD, and Linet MS. Lymphoma incidence patterns by WHO subtype in the United States, 1992-2001. *Blood*. 2006;107(1):265-76.
2. Dave SS, Wright G, Tan B, Rosenwald A, Gascoyne RD, Chan WC, Fisher RI, Braziel RM, Rimsza LM, Grogan TM, et al. Prediction of survival in follicular lymphoma based on molecular features of tumor-infiltrating immune cells. *N Engl J Med*. 2004;351(21):2159-69.
3. Stevenson FK, and Stevenson GT. Follicular lymphoma and the immune system: from pathogenesis to antibody therapy. *Blood*. 2012;119(16):3659-67.
4. Kridel R, Sehn LH, and Gascoyne RD. Pathogenesis of follicular lymphoma. *The Journal of clinical investigation*. 2012;122(10):3424-31.
5. Kahl BS, and Yang DT. Follicular lymphoma: evolving therapeutic strategies. *Blood*. 2016;127(17):2055-63.
6. Gopal AK, Kahl BS, de Vos S, Wagner-Johnston ND, Schuster SJ, Jurczak WJ, Flinn IW, Flowers CR, Martin P, Viardot A, et al. PI3Kdelta inhibition by idelalisib in patients with relapsed indolent lymphoma. *N Engl J Med*. 2014;370(11):1008-18.
7. Pon JR, and Marra MA. Clinical impact of molecular features in diffuse large B-cell lymphoma and follicular lymphoma. *Blood*. 2016;127(2):181-6.
8. Kuppers R, and Stevenson FK. Critical influences on the pathogenesis of follicular lymphoma. *Blood*. 2018;131(21):2297-306.
9. Yildiz M, Li H, Bernard D, Amin NA, Ouilllette P, Jones S, Saiya-Cork K, Parkin B, Jacobi K, Shedden K, et al. Activating STAT6 mutations in follicular lymphoma. *Blood*. 2015;125(4):668-79.
10. Pasqualucci L, Khiabanian H, Fangazio M, Vasishtha M, Messina M, Holmes AB, Ouilllette P, Trifonov V, Rossi D, Tabbo F, et al. Genetics of follicular lymphoma transformation. *Cell reports*. 2014;6(1):130-40.
11. Okosun J, Bodor C, Wang J, Araf S, Yang CY, Pan C, Boller S, Cittaro D, Bozek M, Iqbal S, et al. Integrated genomic analysis identifies recurrent mutations and evolution patterns driving the initiation and progression of follicular lymphoma. *Nature genetics*. 2014;46(2):176-81.
12. Li H, Kaminski MS, Li Y, Yildiz M, Ouilllette P, Jones S, Fox H, Jacobi K, Saiya-Cork K, Bixby D, et al. Mutations in linker histone genes HIST1H1 B, C, D, and E; OCT2 (POU2F2); IRF8; and ARID1A underlying the pathogenesis of follicular lymphoma. *Blood*. 2014;123(10):1487-98.
13. Pasqualucci L, Dominguez-Sola D, Chiarenza A, Fabbri G, Grunn A, Trifonov V, Kasper LH, Lerach S, Tang H, Ma J, et al. Inactivating mutations of acetyltransferase genes in B-cell lymphoma. *Nature*. 2011;471(7337):189-95.
14. Morin RD, Johnson NA, Severson TM, Mungall AJ, An J, Goya R, Paul JE, Boyle M, Woolcock BW, Kuchenbauer F, et al. Somatic mutations altering EZH2 (Tyr641) in follicular and diffuse large B-cell lymphomas of germinal-center origin. *Nature genetics*. 2010;42(2):181-5.
15. Morin RD, Mendez-Lago M, Mungall AJ, Goya R, Mungall KL, Corbett RD, Johnson NA, Severson TM, Chiu R, Field M, et al. Frequent mutation of histone-modifying genes in non-Hodgkin lymphoma. *Nature*. 2011;476(7360):298-303.
16. Green MR, Gentles AJ, Nair RV, Irish JM, Kihira S, Liu CL, Kela I, Hopmans ES, Myklebust JH, Ji H, et al. Hierarchy in somatic mutations arising during genomic evolution and progression of follicular lymphoma. *Blood*. 2013;121(9):1604-11.
17. Ortega-Molina A, Boss IW, Canela A, Pan H, Jiang Y, Zhao C, Jiang M, Hu D, Agirre X, Niesvizky I, et al. The histone lysine methyltransferase KMT2D sustains a gene expression program that represses B cell lymphoma development. *Nature medicine*. 2015;21(10):1199-208.
18. Krysiak K, Gomez F, White BS, Matlock M, Miller CA, Trani L, Fronick CC, Fulton RS, Kreisel F, Cashen AF, et al. Recurrent somatic mutations affecting B-cell receptor signaling pathway genes in follicular lymphoma. *Blood*. 2017;129(4):473-83.

19. Zhang J, Vlasevska S, Wells VA, Nataraj S, Holmes AB, Duval R, Meyer SN, Mo T, Basso K, Brindle PK, et al. The CREBBP Acetyltransferase Is a Haploinsufficient Tumor Suppressor in B-cell Lymphoma. *Cancer discovery*. 2017;7(3):322-37.
20. Boice M, Salloum D, Mourcin F, Sanghvi V, Amin R, Oricchio E, Jiang M, Mottok A, Denis-Lagache N, Ciriello G, et al. Loss of the HVEM Tumor Suppressor in Lymphoma and Restoration by Modified CAR-T Cells. *Cell*. 2016;167(2):405-18 e13.
21. Zhang J, Dominguez-Sola D, Hussein S, Lee JE, Holmes AB, Bansal M, Vlasevska S, Mo T, Tang H, Basso K, et al. Disruption of KMT2D perturbs germinal center B cell development and promotes lymphomagenesis. *Nature medicine*. 2015;21(10):1190-8.
22. Jiang Y, Ortega-Molina A, Geng H, Ying HY, Hatzi K, Parsa S, McNally D, Wang L, Doane AS, Agirre X, et al. CREBBP Inactivation Promotes the Development of HDAC3-Dependent Lymphomas. *Cancer discovery*. 2017;7(1):38-53.
23. McCabe MT, Ott HM, Ganji G, Korenchuk S, Thompson C, Van Aller GS, Liu Y, Graves AP, Della Pietra A, 3rd, Diaz E, et al. EZH2 inhibition as a therapeutic strategy for lymphoma with EZH2-activating mutations. *Nature*. 2012;492(7427):108-12.
24. Okosun J, Wolfson RL, Wang J, Araf S, Wilkins L, Castellano BM, Escudero-Ibarz L, Al Seraihi AF, Richter J, Bernhart SH, et al. Recurrent mTORC1-activating RRAGC mutations in follicular lymphoma. *Nature genetics*. 2016;48(2):183-8.
25. Ying ZX, Jin M, Peterson LF, Bernard D, Saiya-Cork K, Yildiz M, Wang S, Kaminski MS, Chang AE, Klionsky DJ, et al. Recurrent Mutations in the MTOR Regulator RRAGC in Follicular Lymphoma. *Clinical cancer research*: 2016;22(21):5383-93.
26. Oricchio E, Katanayeva N, Donaldson MC, Sungalee S, Pasion JP, Beguelin W, Battistello E, Sanghvi VR, Jiang M, Jiang Y, et al. Genetic and epigenetic inactivation of SESTRIN1 controls mTORC1 and response to EZH2 inhibition in follicular lymphoma. *Science translational medicine*. 2017;9(396).
27. Zoncu R, Bar-Peled L, Efeyan A, Wang S, Sancak Y, and Sabatini DM. mTORC1 senses lysosomal amino acids through an inside-out mechanism that requires the vacuolar H(+)-ATPase. *Science*. 2011;334(6056):678-83.
28. Cotter K, Stransky L, McGuire C, and Forgac M. Recent Insights into the Structure, Regulation, and Function of the V-ATPases. *Trends in biochemical sciences*. 2015;40(10):611-22.
29. Maxson ME, and Grinstein S. The vacuolar-type H(+)-ATPase at a glance - more than a proton pump. *Journal of cell science*. 2014;127(Pt 23):4987-93.
30. Green MR, Kihira S, Liu CL, Nair RV, Salari R, Gentles AJ, Irish J, Stehr H, Vicente-Duenas C, Romero-Camarero I, et al. Mutations in early follicular lymphoma progenitors are associated with suppressed antigen presentation. *Proceedings of the National Academy of Sciences of the United States of America*. 2015;112(10):E1116-25.
31. Anraku Y, Hirata R, Wada Y, and Ohya Y. Molecular genetics of the yeast vacuolar H(+)-ATPase. *The Journal of experimental biology*. 1992;172(67-81).
32. Zhao J, Benlekbir S, and Rubinstein JL. Electron cryomicroscopy observation of rotational states in a eukaryotic V-ATPase. *Nature*. 2015;521(7551):241-5.
33. Liu Q, Kane PM, Newman PR, and Forgac M. Site-directed mutagenesis of the yeast V-ATPase B subunit (Vma2p). *The Journal of biological chemistry*. 1996;271(4):2018-22.
34. Mijaljica D, Prescott M, and Devenish RJ. V-ATPase engagement in autophagic processes. *Autophagy*. 2011;7(6):666-8.
35. Mauvezin C, Nagy P, Juhasz G, and Neufeld TP. Autophagosome-lysosome fusion is independent of V-ATPase-mediated acidification. *Nature communications*. 2015;6(7007).
36. Settembre C, Fraldi A, Medina DL, and Ballabio A. Signals from the lysosome: a control centre for cellular clearance and energy metabolism. *Nature reviews Molecular cell biology*. 2013;14(5):283-96.
37. Yamashiro CT, Kane PM, Wolczyk DF, Preston RA, and Stevens TH. Role of vacuolar acidification in protein sorting and zymogen activation: a genetic analysis of the yeast vacuolar proton-translocating ATPase. *Molecular and cellular biology*. 1990;10(7):3737-49.

38. Jewell JL, Russell RC, and Guan KL. Amino acid signalling upstream of mTOR. *Nature reviews Molecular cell biology*. 2013;14(3):133-9.
39. Kabeya Y, Mizushima N, Ueno T, Yamamoto A, Kirisako T, Noda T, Kominami E, Ohsumi Y, and Yoshimori T. LC3, a mammalian homologue of yeast Apg8p, is localized in autophagosome membranes after processing. *The EMBO journal*. 2000;19(21):5720-8.
40. Tanida I, Minematsu-Ikeguchi N, Ueno T, and Kominami E. Lysosomal turnover, but not a cellular level, of endogenous LC3 is a marker for autophagy. *Autophagy*. 2005;1(2):84-91.
41. Mizushima N, Yoshimori T, and Levine B. Methods in mammalian autophagy research. *Cell*. 2010;140(3):313-26.
42. Huang WP, Scott SV, Kim J, and Klionsky DJ. The itinerary of a vesicle component, Aut7p/Cvt5p, terminates in the yeast vacuole via the autophagy/Cvt pathways. *The Journal of biological chemistry*. 2000;275(8):5845-51.
43. Kanki T, Wang K, Baba M, Bartholomew CR, Lynch-Day MA, Du Z, Geng J, Mao K, Yang Z, Yen WL, et al. A genomic screen for yeast mutants defective in selective mitochondria autophagy. *Molecular biology of the cell*. 2009;20(22):4730-8.
44. Valvezan AJ, Turner M, Belaid A, Lam HC, Miller SK, McNamara MC, Baglini C, Housden BE, Perrimon N, Kwiatkowski DJ, et al. mTORC1 Couples Nucleotide Synthesis to Nucleotide Demand Resulting in a Targetable Metabolic Vulnerability. *Cancer cell*. 2017;32(5):624-38 e5.
45. Ben-Sahra I, and Manning BD. mTORC1 signaling and the metabolic control of cell growth. *Current opinion in cell biology*. 2017;45(72-82).
46. Menon S, Dibble CC, Talbott G, Hoxhaj G, Valvezan AJ, Takahashi H, Cantley LC, and Manning BD. Spatial control of the TSC complex integrates insulin and nutrient regulation of mTORC1 at the lysosome. *Cell*. 2014;156(4):771-85.
47. Wyant GA, Abu-Remaileh M, Wolfson RL, Chen WW, Freinkman E, Danai LV, Vander Heiden MG, and Sabatini DM. mTORC1 Activator SLC38A9 Is Required to Efflux Essential Amino Acids from Lysosomes and Use Protein as a Nutrient. *Cell*. 2017;171(3):642-54 e12.
48. Abu-Remaileh M, Wyant GA, Kim C, Laqtom NN, Abbasi M, Chan SH, Freinkman E, and Sabatini DM. Lysosomal metabolomics reveals V-ATPase- and mTOR-dependent regulation of amino acid efflux from lysosomes. *Science*. 2017;358(6364):807-13.
49. Sancak Y, Peterson TR, Shaul YD, Lindquist RA, Thoreen CC, Bar-Peled L, and Sabatini DM. The Rag GTPases bind raptor and mediate amino acid signaling to mTORC1. *Science*. 2008;320(5882):1496-501.
50. Kim E, Goraksha-Hicks P, Li L, Neufeld TP, and Guan KL. Regulation of TORC1 by Rag GTPases in nutrient response. *Nature cell biology*. 2008;10(8):935-45.
51. Beck T, and Hall MN. The TOR signalling pathway controls nuclear localization of nutrient-regulated transcription factors. *Nature*. 1999;402(6762):689-92.
52. Kamada Y, Funakoshi T, Shintani T, Nagano K, Ohsumi M, and Ohsumi Y. Tor-mediated induction of autophagy via an Apg1 protein kinase complex. *The Journal of cell biology*. 2000;150(6):1507-13.
53. Schmidt A, Beck T, Koller A, Kunz J, and Hall MN. The TOR nutrient signalling pathway phosphorylates NPR1 and inhibits turnover of the tryptophan permease. *The EMBO journal*. 1998;17(23):6924-31.
54. B'Chir W, Maurin AC, Carraro V, Averous J, Jousse C, Muranishi Y, Parry L, Stepien G, Fafournoux P, and Bruhat A. The eIF2alpha/ATF4 pathway is essential for stress-induced autophagy gene expression. *Nucleic acids research*. 2013;41(16):7683-99.
55. Bernard A, Jin M, Xu Z, and Klionsky DJ. A large-scale analysis of autophagy-related gene expression identifies new regulators of autophagy. *Autophagy*. 2015;11(11):2114-22.
56. Yao Z, Delorme-Axford E, Backues SK, and Klionsky DJ. Atg41/Icy2 regulates autophagosome formation. *Autophagy*. 2015;11(12):2288-99.
57. Yu L, McPhee CK, Zheng L, Mardones GA, Rong Y, Peng J, Mi N, Zhao Y, Liu Z, Wan F, et al. Termination of autophagy and reformation of lysosomes regulated by mTOR. *Nature*. 2010;465(7300):942-6.

58. Rebsamen M, Pochini L, Stasyk T, de Araujo ME, Galluccio M, Kandasamy RK, Snijder B, Fauster A, Rudashevskaya EL, Bruckner M, et al. SLC38A9 is a component of the lysosomal amino acid sensing machinery that controls mTORC1. *Nature*. 2015;519(7544):477-81.
59. Jung J, Genau HM, and Behrends C. Amino Acid-Dependent mTORC1 Regulation by the Lysosomal Membrane Protein SLC38A9. *Molecular and cellular biology*. 2015;35(14):2479-94.
60. Wang S, Tsun ZY, Wolfson RL, Shen K, Wyant GA, Plovonich ME, Yuan ED, Jones TD, Chantranupong L, Comb W, et al. Metabolism. Lysosomal amino acid transporter SLC38A9 signals arginine sufficiency to mTORC1. *Science*. 2015;347(6218):188-94.
61. Hughes AL, and Gottschling DE. An early age increase in vacuolar pH limits mitochondrial function and lifespan in yeast. *Nature*. 2012;492(7428):261-5.
62. McGuire CM, and Forgac M. Glucose starvation increases V-ATPase assembly and activity in mammalian cells through AMP kinase and phosphatidylinositide 3-kinase/Akt signaling. *The Journal of biological chemistry*. 2018;293(23):9113-23.
63. Kane PM. Disassembly and reassembly of the yeast vacuolar H(+)-ATPase in vivo. *The Journal of biological chemistry*. 1995;270(28):17025-32.
64. Egan DF, Chun MG, Vamos M, Zou H, Rong J, Miller CJ, Lou HJ, Raveendra-Panickar D, Yang CC, Sheffler DJ, et al. Small Molecule Inhibition of the Autophagy Kinase ULK1 and Identification of ULK1 Substrates. *Molecular cell*. 2015;59(2):285-97.
65. Petherick KJ, Conway OJ, Mpamhanga C, Osborne SA, Kamal A, Saxty B, and Ganley IG. Pharmacological inhibition of ULK1 kinase blocks mammalian target of rapamycin (mTOR)-dependent autophagy. *The Journal of biological chemistry*. 2015;290(48):28726.
66. Kaizuka T, Morishita H, Hama Y, Tsukamoto S, Matsui T, Toyota Y, Kodama A, Ishihara T, Mizushima T, and Mizushima N. An Autophagic Flux Probe that Releases an Internal Control. *Molecular cell*. 2016;64(4):835-49.
67. Su H, Yang F, Wang Q, Shen Q, Huang J, Peng C, Zhang Y, Wan W, Wong CCL, Sun Q, et al. VPS34 Acetylation Controls Its Lipid Kinase Activity and the Initiation of Canonical and Non-canonical Autophagy. *Molecular cell*. 2017;67(6):907-21 e7.
68. Milkereit R, Persaud A, Vanoaica L, Guetg A, Verrey F, and Rotin D. LAPTM4b recruits the LAT1-4F2hc Leu transporter to lysosomes and promotes mTORC1 activation. *Nature communications*. 2015;6(7250).
69. Rebecca VW, Nicastrì MC, McLaughlin N, Fennelly C, McAfee Q, Ronghe A, Nofal M, Lim CY, Witze E, Chude CI, et al. A Unified Approach to Targeting the Lysosome's Degradative and Growth Signaling Roles. *Cancer discovery*. 2017;7(11):1266-83.
70. Gayle S, Landrette S, Beeharry N, Conrad C, Hernandez M, Beckett P, Ferguson SM, Mandelkern T, Zheng M, Xu T, et al. Identification of apilimod as a first-in-class PIKfyve kinase inhibitor for treatment of B-cell non-Hodgkin lymphoma. *Blood*. 2017;129(13):1768-78.
71. Lazarus MB, Novotny CJ, and Shokat KM. Structure of the human autophagy initiating kinase ULK1 in complex with potent inhibitors. *ACS chemical biology*. 2015;10(1):257-61.
72. Ross CW, Ouillette PD, Saddler CM, Shedden KA, and Malek SN. Comprehensive analysis of copy number and allele status identifies multiple chromosome defects underlying follicular lymphoma pathogenesis. *Clinical cancer research* : 2007;13(16):4777-85.
73. Galban S, Hwang C, Rumble JM, Oetjen KA, Wright CW, Boudreault A, Durkin J, Gillard JW, Jaquith JB, Morris SJ, et al. Cytoprotective effects of IAPs revealed by a small molecule antagonist. *Biochem J*. 2009;417(3):765-71.
74. Peterson LF, Wang Y, Lo MC, Yan M, Kanbe E, and Zhang DE. The multi-functional cellular adhesion molecule CD44 is regulated by the 8;21 chromosomal translocation. *Leukemia*. 2007;21(9):2010-9.
75. Sanjana NE, Shalem O, and Zhang F. Improved vectors and genome-wide libraries for CRISPR screening. *Nature methods*. 2014;11(8):783-4.

76. Longtine MS, McKenzie A, 3rd, Demarini DJ, Shah NG, Wach A, Brachat A, Philippsen P, and Pringle JR. Additional modules for versatile and economical PCR-based gene deletion and modification in *Saccharomyces cerevisiae*. *Yeast*. 1998;14(10):953-61.
77. Toulmay A, and Schneider R. A two-step method for the introduction of single or multiple defined point mutations into the genome of *Saccharomyces cerevisiae*. *Yeast*. 2006;23(11):825-31.
78. Gueldener U, Heinisch J, Koehler GJ, Voss D, and Hegemann JH. A second set of loxP marker cassettes for Cre-mediated multiple gene knockouts in budding yeast. *Nucleic acids research*. 2002;30(6):e23.
79. Li C, Wen A, Shen B, Lu J, Huang Y, and Chang Y. FastCloning: a highly simplified, purification-free, sequence- and ligation-independent PCR cloning method. *BMC biotechnology*. 2011;11(92).
80. Liu H, and Naismith JH. An efficient one-step site-directed deletion, insertion, single and multiple-site plasmid mutagenesis protocol. *BMC biotechnology*. 2008;8(91).
81. Shintani T, and Klionsky DJ. Cargo proteins facilitate the formation of transport vesicles in the cytoplasm to vacuole targeting pathway. *The Journal of biological chemistry*. 2004;279(29):29889-94.
82. Noda T, and Klionsky DJ. The quantitative Pho8Delta60 assay of nonspecific autophagy. *Methods in enzymology*. 2008;451(33-42).
83. Hu G, McQuiston T, Bernard A, Park YD, Qiu J, Vural A, Zhang N, Waterman SR, Blewett NH, Myers TG, et al. A conserved mechanism of TOR-dependent RCK-mediated mRNA degradation regulates autophagy. *Nature cell biology*. 2015;17(7):930-42.

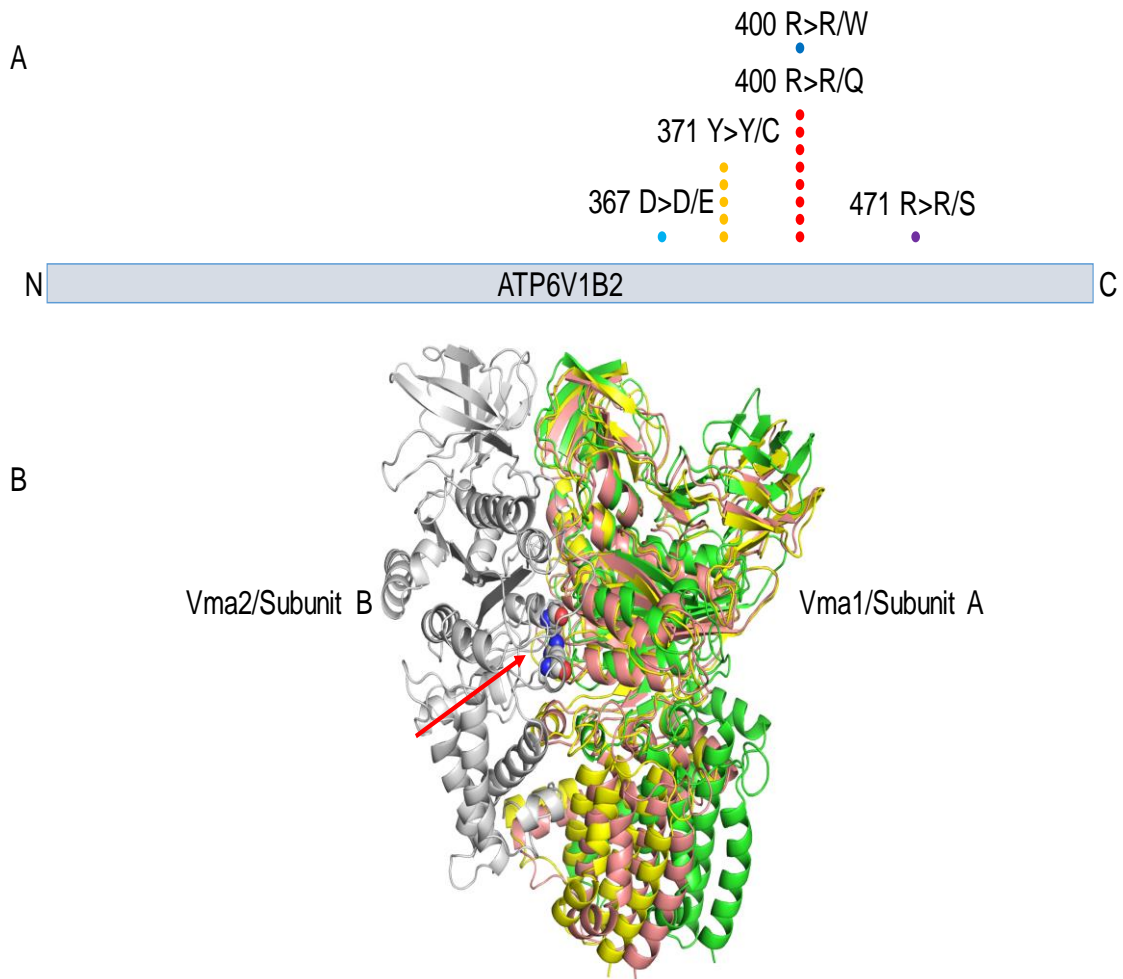


Figure 1: Graphical display and 3D modeling of follicular lymphoma (FL)-associated ATP6V1B2 (v-ATPase) mutations.

A: *ATP6V1B2* mutations at known hotspots (p.Y371Y>C and p.R400R>Q) and novel mutations identified in this study are indicated.

B: 3-D model of yeast v-ATPase based on EM data published by Zhao et al, Nature 2015 (32). The location of yeast amino acid residues corresponding to human ATP6V1B2 hotspot mutations p.Y371Y>C and p.R400R>Q are indicated by the red arrow. The mutations are located in a region of yeast Vma2/v-ATPase subunit B, which are involved in the ability of the complex to adopt different functional states (green: open; pink: loose; yellow: tight; all three states are superimposed in this figure).

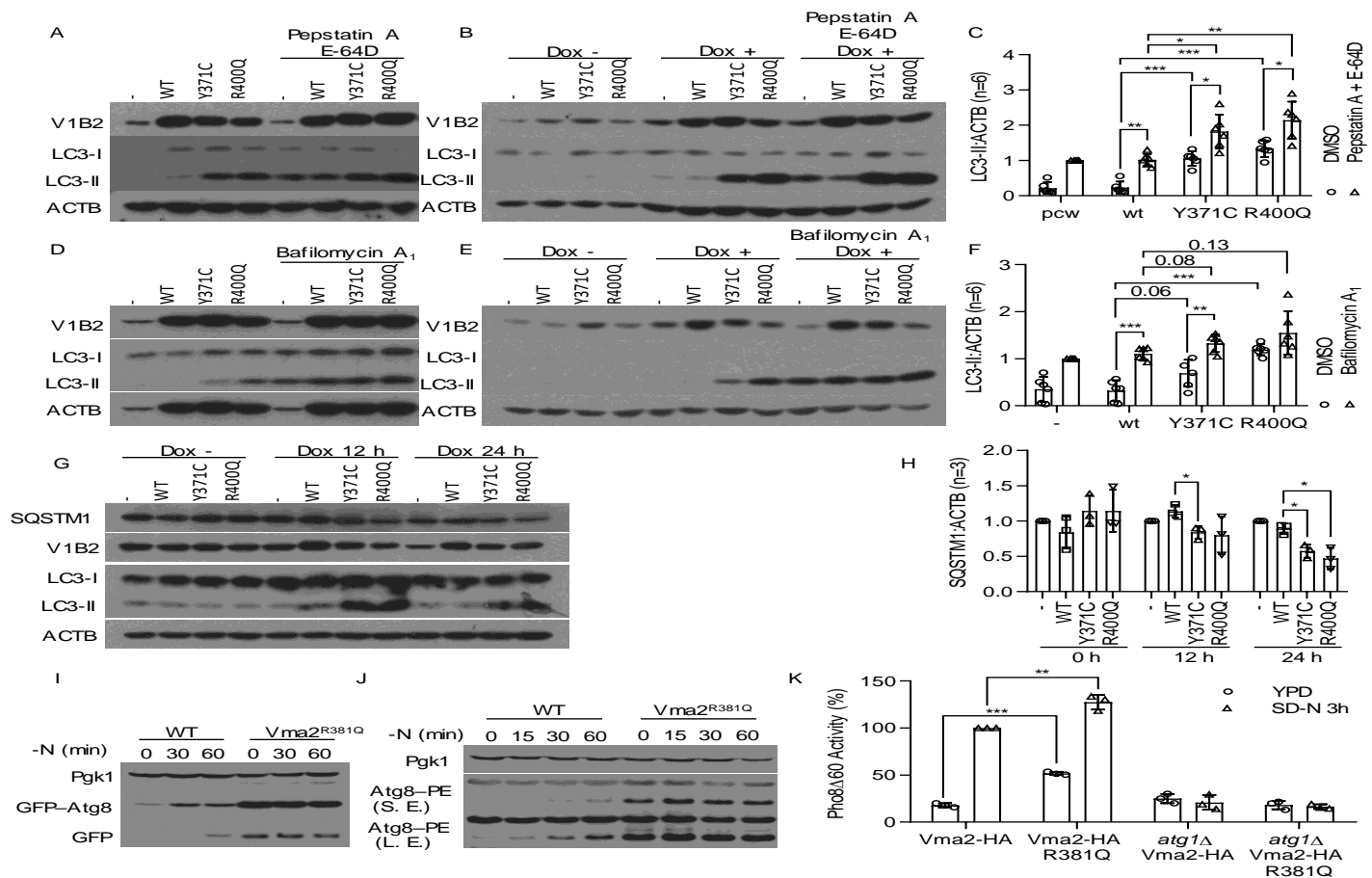


Figure 2: Follicular lymphoma-associated ATP6V1B2 mutations activate autophagic flux.

A: HEK293T cells transfected with empty vector, WT or mutant (Y371; R400Q) ATP6V1B2 treated with/without pepstatin A/E-64d.

B: Stable OCI-LY1 lymphoma cells carrying an inducible lentivirus (pCW57.1) expressing WT or mutated ATP6V1B2 (-/+ doxycycline) treated with/without pepstatin A/E-64d.

C: Densitometry quantification (LC3-II:ACTB) of three independent experiments per cell line from representative panels A and B. Statistical comparisons: i) R400Q or Y371C versus WT (A; lanes 2-4; B: lanes 6-8); ii) R400Q or Y371C versus WT plus pepstatin A/E-64D (A; lanes 6-8; B: lanes 10-12); iii) R400Q or Y371C or WT +/- pepstatin A/E-64D. **C, F and H:** Comparisons using unpaired 2-tailed t-testing and Bonferroni corrections. * p<0.05; ** p<0.01, *** p< 0.001). Bars: Standard Deviations.

D: HEK293T cells as in panel A treated +/- bafilomycin A₁.

E: Stable OCI-LY1 lymphoma cells as in panel B (-/+ doxycycline) treated +/- bafilomycin A₁.

F: Densitometry quantification (LC3-II:ACTB) of three independent experiments per cell line from representative panels D and E. Statistical comparisons: i) R400Q or Y371C versus WT (A; lanes 2-4; B: lanes 6-8); ii) R400Q or Y371C versus WT plus bafilomycin A₁ (A; lanes 6-8; B: lanes 10-12); iii) R400Q or Y371C or WT +/- bafilomycin A₁.

G: Stable HEK293T cells carrying inducible WT or mutated ATP6V1B2 induced with doxycycline for 12 or 24 h.

H: Densitometry quantification (SQSTM1:ACTB) of three independent experiments from panel G (*p<0.05, R400Q or Y371C versus WT comparisons within time points).

I-K: *S. cerevisiae* strain WLY176 was used to generate a Vma2^{R381Q}-HA knock-in point mutation in the genome. Autophagy activity was measured +/- nitrogen using **I:** GFP-Atg8 processing assay; **J:** Atg8 lipidation assay; **K:** Pho8Δ60 activity assay. Comparisons using unpaired 2-tailed t-testing ** p<0.01, *** p< 0.001. Bars: Standard Deviations.

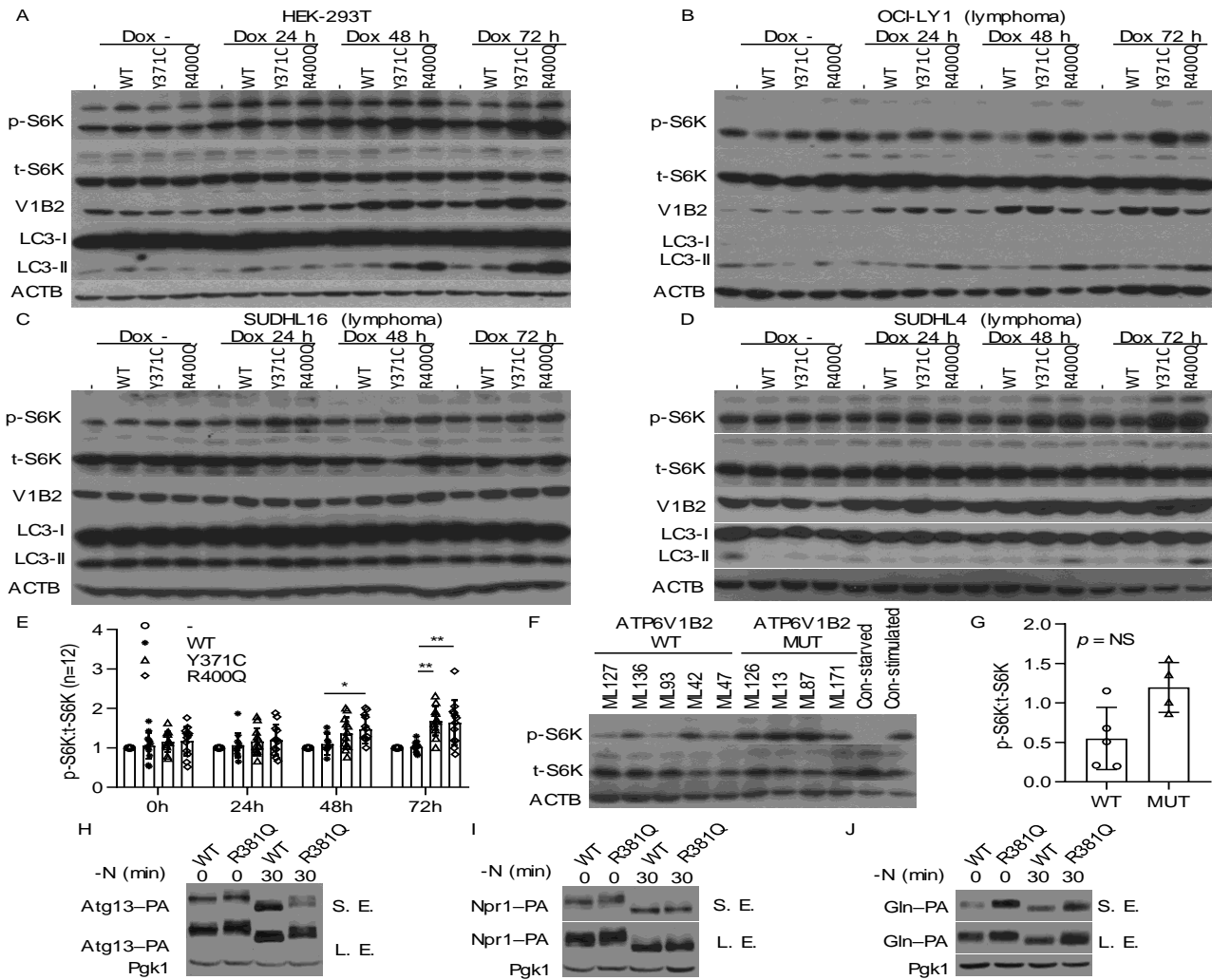


Figure 3: Follicular lymphoma-associated ATP6V1B2 mutations activate both autophagic flux and MTOR.

A: Stable HEK293T cells carrying the inducible lentivirus pCW57.1 with WT or mutated (Y371; R400Q) ATP6V1B2. Cells were induced with doxycycline for 0, 24, 48 or 72 h.

B-D: Stable OCI-LY1, SUDHL16 or SUDHL4 lymphoma cells carrying the inducible lentivirus pCW57.1 with WT or mutated (Y371; R400Q) ATP6V1B2. Cells were induced with doxycycline for 0, 24, 48 or 72 h. Delayed activation of MTOR as evidenced by elevated p-RPS6KB:S6K levels is detected.

E: Combined densitometry quantification (p-RPS6KB:S6K) of three independent experiments per cell line from panels A-D (* $p < 0.05$; ** $p < 0.01$; R400Q or Y371C versus WT comparisons within time points using unpaired 2-tailed t-testing and Bonferroni corrections). Bars: Standard Deviations.

F-G: Phosphorylation of RPS6KB in purified primary human Follicular Lymphoma B cells carrying wild type or mutated ATP6V1B2.

F: immunoblot results of lysates from 5 purified FL B cell cases carrying wild type ATP6V1B2 and four purified FL B cell cases carrying mutated ATP6V1B2 and control lysates made from unstimulated or insulin/serum stimulated OCI-LY7 cells. One of two representative immunoblots is shown.

G: densitometry quantification (p-RPS6KB:S6K) of blots shown in panel G. Bars: Standard Deviations.

H-J: Tor activity measured by phosphorylation in *S. cerevisiae* in growing conditions and after 30 min nitrogen starvation (substrate gel migration assay; the higher the phosphorylation state the slower the gel migration) for

H: Atg13; **I:** Npr1; **J:** Gln3. Varying exposure times are shown.

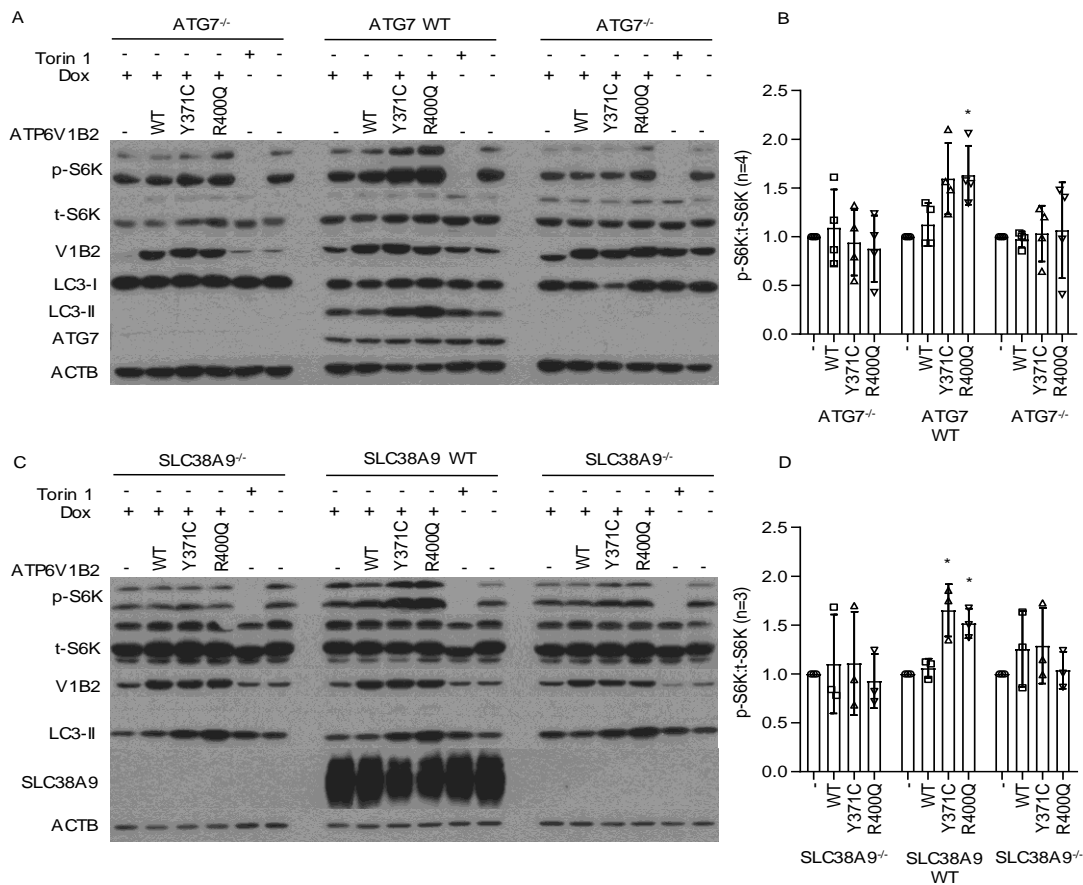


Figure 4: An intact autophagy pathway and lysosomal amino acid sensing/transport are necessary for delayed activation of MTOR by mutant ATP6V1B2.

A-B: *ATG7*^{-/-} HEK293T were generated using crispr-Cas9 targeting and independent single cell clones expanded. Control *ATG7* wild type cells were expanded from cells that were subjected to crispr-Cas9 targeting but remained *ATG7* intact. All clones were subsequently infected with lentiviruses carrying doxycycline-inducible ATP6V1B2 wild type or mutants. Cells were induced with doxycycline for 72h and cell lysates prepared for immunoblotting using the indicated antibodies.

B: Results of quantification (p-RPS6KB:S6K) of four independent experiments using data from all lanes labeled WT, Y371C and R400Q. Statistical analysis compared the difference of the differences between measurements under *ATG7* WT and *ATG7*^{-/-} conditions (see methods). P=0.06 for Y371C and p=0.04 for R400Q for *ATG7*^{-/-}/*ATG7* comparisons. Bars: Standard Deviations.

C-D: *SLC38A9*^{-/-} HEK293T were generated using crispr-Cas9 targeting and independent single cell clones expanded. Control *SLC38A9* wild type cells were expanded from cells that were subjected to crispr-Cas9 targeting but remained *SLC38A9* intact. All clones were infected with lentiviruses carrying doxycycline-inducible ATP6V1B2 wild type or mutants. Cells were induced with doxycycline for 72h and cell lysates prepared for immunoblotting using the indicated antibodies.

D: Results of quantification (p-RPS6KB:S6K) of three independent experiments using data from all lanes labeled WT, Y371C and R400Q. Statistical analysis compared the difference of the differences between measurements under *SLC38A9* WT and *SLC38A9*^{-/-} conditions (see methods). P=0.01 for Y371C and p=0.01 for R400Q for *SLC38A9*^{-/-}/*SLC38A9* comparisons. Bars: Standard Deviations.

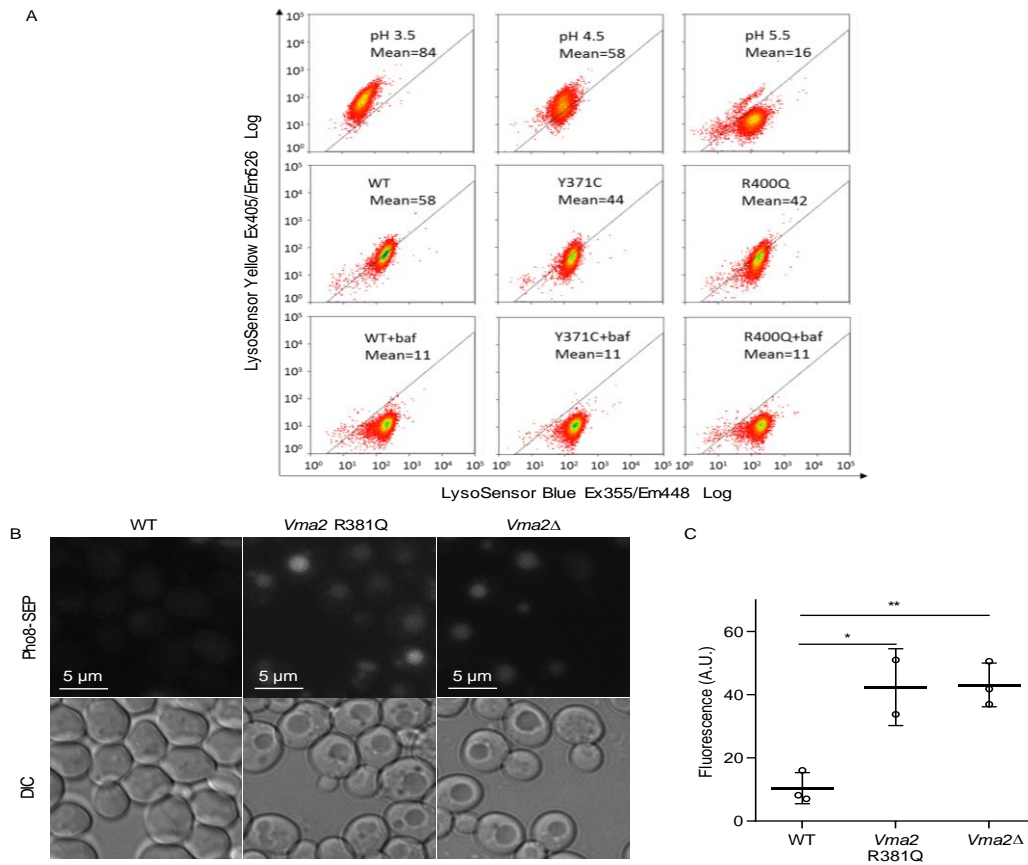


Figure 5: Follicular lymphoma-associated ATP6V1B2 mutations reduce the ability of the v-ATPase to acidify lysosomes.

A: Stable HEK293T cells were generated using the doxycycline-inducible lentivirus pCW57.1 carrying WT or mutated cDNAs encoding ATP6V1B2. Cells were induced with doxycycline for 48 h and afterwards loaded with a pH indicator dye (dextran-conjugated LysoSensor Blue/Yellow) for 12 h. In parallel, untransfected HEK293T cells were treated with EMS buffer (see methods) calibrated to pH 3.5, pH 4.5 or pH 5.5 serving as pH controls. The fluorescence intensity of cell suspensions was read at various wavelengths using flow cytometry. The mean fluorescence intensity of the yellow dye fluorescence signal is a measure of lysosomal pH. Bafilomycin A₁ which completely blocks lysosomal acidification, was used as a control for neutral pH.

B: In *S. cerevisiae*, the C terminus of the protein Pho8 was tagged with a pH-sensitive Super Ecliptic pFluorin (SEP) protein that increases fluorescence with increasing pH. Similar to *vma2*Δ (a knockout strain of the yeast homolog of human ATP6V1B2), *Vma2*^{R381Q} cells demonstrated increased vacuolar pH compared to wild-type cells. LEFT pictures: fluorescence signal; RIGHT pictures: corresponding light microscopy.

C: Summary of the fluorescence intensity (A.U., arbitrary units) of vacuolar fluorescence measurements in *S. cerevisiae* of the data in panel B. Comparisons using t-testing and Bonferroni corrections; *p<0.05; **p<0.01. Standard deviations are plotted.

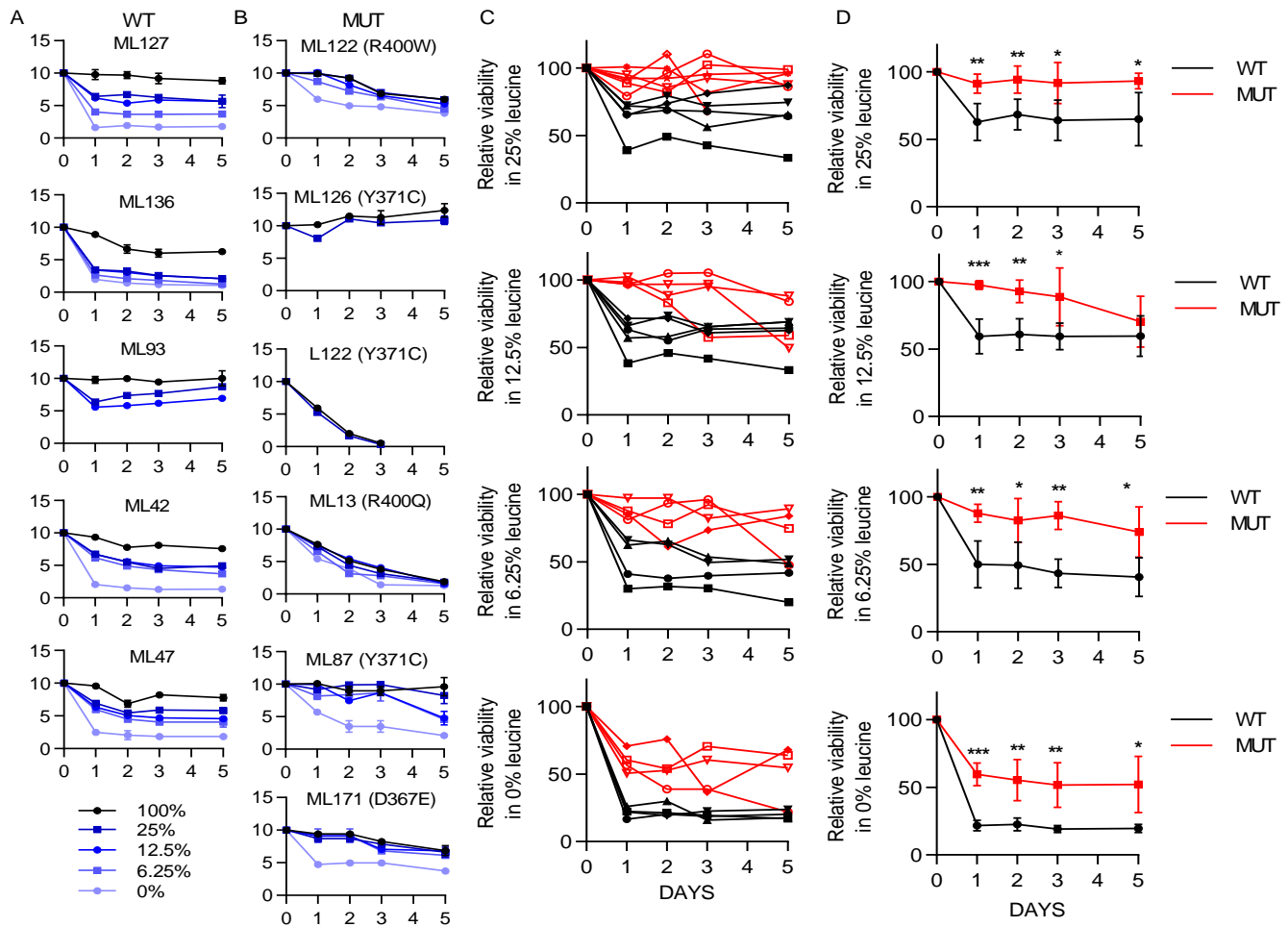


Figure 6: Follicular lymphoma-associated *ATP6V1B2* mutations increase the viability of primary human FL B cells under leucine starvation conditions. Purified FL B cells carrying **A:** wild type (N=5) or **B:** mutant (N=6) *ATP6V1B2* were cultured in dialyzed serum-supplemented RPMI1640 medium containing either 100% leucine (Leu) or depending on the availability of sufficient cells reduced Leu concentrations (0, 6.25, 12.5 and 25%). FL B cells were cultured and the cell number and fraction of living cells determined for up to 5 days. Y-axis: relative cell numbers; X-axis: days.

C-D: Summary results of the individual data displayed in panels **A** and **B**. Displayed is the number of viable cells at various Leu concentrations divided by the number of living cells at 100% Leu. Significance levels are indicated by asterisks: (** p<0.01, ***p<0.001; compared to results for wild type at the same time point; comparisons were done with t-testing). Standard deviations are plotted. Black: WT; Red: mutant *ATP6V1B2*.

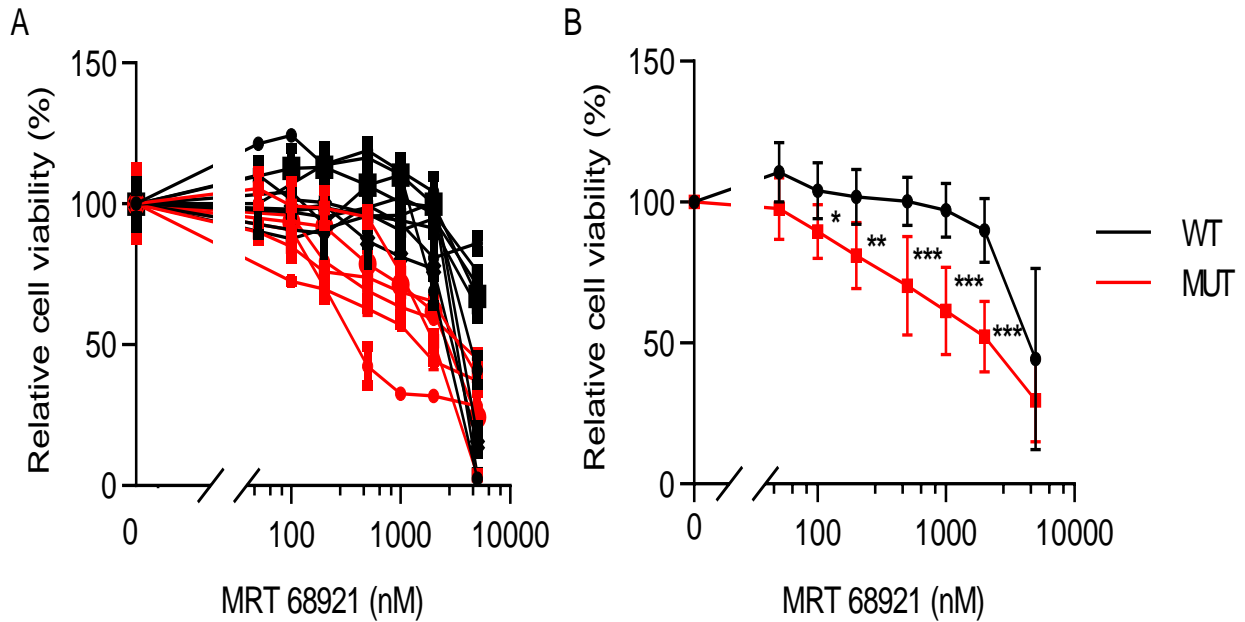


Figure 7: Follicular lymphoma-associated *ATP6V1B2* mutations and dependence on autophagic flux for survival of primary FL B cells: A-B: Primary human purified FL B cells carrying wild type or mutant *ATP6V1B2* were cultured in serum-supplemented RPMI1640 medium containing 100% Leu and treated with the ULK1 inhibitor MRT68921 for 72 h at the indicated concentrations. Cell viability was measured using Celltiter-Glo® and is displayed normalized to the viability of cells cultured for 72 h but left untreated. Red: mutant *ATP6V1B2*; Black: wild type *ATP6V1B2*. * p < 0.05, ** p < 0.01, *** p < 0.001 comparisons with results for wild type at the same time point, comparison was done with t-testing. Standard deviations are plotted.